Supplement of Geosci. Model Dev., 19, 5423–5438, 2026
https://doi.org/10.5194/gmd-19-5423-2026-supplement

Geoscientific Model Development Open Access EGU

Supplement of

Rederivation of the centroid formulation in a second-order conservative remapping scheme on spherical coordinates

Fuyuki Saito

Correspondence to: Fuyuki Saito (saitofuyuki@jamstec.go.jp)

S1 Supplementary description of the second-order remapping methods

This supplementary section describes the basic idea of the second-order conservative remapping scheme of Dukowicz and Kodis (1987) (hereafter referred to as DK87), and its extension to the spherical coordinate system as formulated by Jones (1999) (similarly as J99), with supplementary explanation by Jones (2024) (J24). The original equations and terms are transformed into the formulation shown in J99. For example, the volume integral notation in DK87 is replaced by the surface integral in accordance with J99. Additionally, some new symbols unique to the present paper are introduced for description.

It is worth mentioning that the derivation of extension of J99 and thus this study is performed entirely within the latitude-longitude coordinate chart. Modern conservative remapping frameworks (e.g. Hanke et al., 2016; Ullrich and Taylor, 2015; Ullrich et al., 2016) avoid relying on latitude-longitude formulas and instead express all geometry in 3-D Cartesian coordinates.

Hereafter, Eq. (e) in J99 are referred to as Eq. (J99.e) in order to avoid confusion. Also, equations in the main text are referred to as Eq. (Me), while those in this supplement are as Eq. (Se).

S1.1 Derivation on a general case

Below is the set of equations derived in a slightly different way, partially following the DK87 method. The derivation is somewhat roundabout but is necessary for the flow of the present paper. Some trivial descriptions are included so as to avoid ambiguities, which the author believes is necessary in the context of the present paper.

The object is to compute in a conservative manner, a flux term on a destination grid from the flux term on a source grid over a surface of three-dimensional Euclidean space. For any flux terms that must satisfy a constraint to preserve conservation, the flux integral over each source grid cell must be consistent with the average value in the grid cell as follows:

$$\overline{f}_n A_n = \int_{A_n} f_n \, \mathrm{d}A, \tag{S1}$$

where n is the source cell index, f_n and $\overline{f}_n$ are a flux term and its average over the area of source cell n, respectively. Equation (S1) corresponds to Eq. (19) in DK87. Also, Eq. (S1) is identical to Eq. (J99.4).

DK87 proposes to approximate the source flux by a combination of the average and its gradient, with assuming the flux gradient is constant across a source grid cell locally, as follows:

$$f_n = \overline{f}_n + \nabla_n f \cdot (\mathbf{r} - \mathbf{c}_n), \tag{S2}$$

where $\mathbf{r}$ is the position vector, $\mathbf{c}_n$ is the position vector of a reference point (corresponding to $\bar{\mathbf{r}}_k$ in DK87, Eq. 20) and $\nabla_n f$ is a gradient of f in source grid cell n. As mentioned in DK87, Eq. (S2) is equivalent to the first two terms in the Taylor series expansion of f about the point $\mathbf{c}_n$, if it is assumed that the average $\overline{f}_n$ is located at the reference point and if the term $\nabla_n f$ is at least a first order approximation to the gradient. However, the formulation is actually chosen independently of the Taylor expansion among a number of possible solutions which satisfies the conservation characteristics (J24). The reference $\mathbf{c}_n$ can be chosen arbitrarily in the source cell; here, it is defined such that the flux approximation Eq. (S2) satisfies the condition Eq. (S1). By substituting f_n, the following condition is obtained:

$$\overline{f}_n A_n = \overline{f}_n A_n + \int_{A_n} \nabla_n f \cdot (\mathbf{r} - \mathbf{c}_n) \, \mathrm{d}A. \tag{S3}$$

In order to satisfy Eq. (S3) for any flux and its gradient, the following constraint is obtained:

$$\text{(S4)} \qquad \int_{A_n} \nabla_n f \cdot (\mathbf{r} - \mathbf{c}_n)\, \mathrm{d}A = 0.$$

Given a constant gradient across source grid cell n, the gradient terms in Eq. (S4) can be taken out of the integral, and the condition is simplified as follows:

$$\text{(M3)} \qquad \int_{A_n} \mathbf{r}\, \mathrm{d}A - \int_{A_n} \mathbf{c}_n\, \mathrm{d}A = 0.$$

Equation (M3) is the principle condition of the reference $\mathbf{c}_n$ term. Under Eq. (M3) constraints, the flux approximation (Eq. S2) automatically satisfies the conservation characteristics of Eq. (S1). Conservation is preserved with second-order accuracy if the gradient is at least a first-order approximation; if the second term is neglected, the method corresponds to the first-order method.

At least over the three-dimensional Cartesian coordinate system, $\mathbf{c}_n$ term can be taken out of the integral also. In this case, the reference $\mathbf{c}_n$ can be inverted as

$$\text{(M4)} \qquad \mathbf{c}_n = \int_{A_n} \mathbf{r}\, \mathrm{d}A \Big/ \int_{A_n} \mathrm{d}A = \frac{1}{A_n} \int_{A_n} \mathbf{r}\, \mathrm{d}A,$$

which is identical to the formulation of $\bar{\mathbf{r}}_k$ in DK87, and to $\mathbf{r}_n$ in Eq. (J99.6). The position computed in Eq. (M3) or Eq. (M4) corresponds to the geometric center, often referred to as the *centroid*, of the source grid cell n under the geometry of the target Euclidean space. In the derivation of DK87, the term centroid is used to label the reference point before the condition in Eq. (M3) is presented. While this is viable, the author believes it to be slightly more natural to first describe the condition of the reference point and to subsequently describe its coincidence to the centroid, at least in the context of the present study. Such a derivation is also given in the next section.

The position provided by Eq. (M4) is by definition the geometric mass centroid, that lies *inside* the sphere when the cell area A_n is on the surface. Chen et al. (2026) summarize a variation of 'face centerpoints' and provide formulas for the mass centroid, which help to clarify the distinction between the coordinate-invariant mass centroid of a spherical face and the metric-weighted reference coordinate introduced in this study. This point will be revisited later.

S1.2 Extension to spherical coordinates

Extension to the spherical coordinates requires to replace the gradient and displacement terms in Eq. (S2) in the coordinate system. J99 assumes that the gradient term is fixed with the formulation as follows:

$$\text{(S5)} \qquad \nabla_n f = \left(\frac{\partial f}{\partial \theta}\right)_n \hat{\theta} + \left(\frac{1}{\cos\theta}\frac{\partial f}{\partial \phi}\right)_n \hat{\phi},$$

where symbols θ and ϕ are adopted for the latitude and longitude coordinates, respectively (J24). The position vector $\mathbf{r} = [x, y, z]^\mathsf{T}$ of the Cartesian coordinate on the unit sphere is expressed using the spherical coordinate components $(\hat{\theta}, \hat{\phi})$ which depend on θ and ϕ. The inner product on the spherical coordinate is not simply a component-wise product as in Cartesian coordinates because the direction of the unit vectors depends on the position. Modern implementations(e.g. Ullrich et al., 2009) formulate Eq. (S5) in terms of three-dimensional Euclidean space that makes all inner products coordinate-invariant. More recently, Chen et al. (2026) provide formulas for the mass centroid with boundary-integral expressions for great-circle polygons and correction terms for constant-latitude edges. In contrast, J99 instead maintains the formulation on the spherical coordinate. J99 approximates that the unit vectors are aligned over the source cell

such that local orthogonality holds true for a simple approach. The local displacement at the coordinate $(\hat{\theta}, \hat{\phi})$ on the unit sphere can be formulated as

$$\mathrm{d}\,\mathbf{r} = \hat{\theta}\ \mathrm{d}\,\theta + \hat{\phi}\cos\theta\ \mathrm{d}\,\phi. \tag{S6}$$

As described above, the geometric mass centroid $\mathbf{c}_n$ does not lie on the surface of the sphere, therefore displacement of a coordinate from the centroid strictly requires a radial component $(\hat{\rho}\ \mathrm{d}\,\rho)$. The above assumption, adopted in J99, corresponds to the idea that the effect of this component is small enough to be ignored. Formally, this assumption can be interpreted as the interior centroid being projected onto the surface of the sphere, with the subsequent remapping being derived along the surface.

Introducing Eq. (S6) at the position $\mathbf{c}_n$ and the gradient term Eq. (S5) into Eq. (S2), the flux term can be approximated as:

$$f_n = \overline{f}_n + \left(\frac{\partial f}{\partial \theta}\right)_n (\theta - \theta_c) + \left(\frac{1}{\cos\theta}\frac{\partial f}{\partial \phi}\right)_n \cos\theta(\phi - \phi_c), \tag{S7}$$

where the coordinates $\mathbf{c}_n = [\rho_c, \theta_c, \phi_c]^{\mathsf{T}}$, or formally, $\mathbf{c}_n = [\theta_c, \phi_c]^{\mathsf{T}}$.

The formulation of J99 is mainly derived for the area-averaged flux over the destination grid cell (after remapping), and is essentially the same as that over the source grid cell. The flux over the destination grid is formulated as follows:

$$\overline{F}_k = \frac{1}{A_k}\sum_{n=1}^{N}\int_{A_{nk}} f_n\ \mathrm{d}A, \tag{S8}$$

where $\overline{F}_k$ is the average flux over the destination grid cell k, and A_{nk} is the area of the source grid cell n covered by the destination grid cell k. The summation is performed for all overlapped cells of N. The average flux term at the destination grid cell can be approximated with using the flux approximation of Eq. (S7), as follows:

$$\overline{F}_k = \sum_{n=1}^{N}\left[\overline{f}_n w_{1\,nk} + \left(\frac{\partial f}{\partial \theta}\right)_n w_{2\,nk} + \left(\frac{1}{\cos\theta}\frac{\partial f}{\partial \phi}\right)_n w_{3\,nk}\right], \tag{S9}$$

which corresponds to Eq. (J99.7). The three coefficients, $w_{1\,nk}$, $w_{2\,nk}$, $w_{3\,nk}$, are called the remapping weights and are derived according to J99 as follows:

$$w_{1\,nk} = \frac{1}{A_k}\int_{A_{nk}} \mathrm{d}A, \tag{S10}$$

$$w_{2\,nk} = \frac{1}{A_k}\int_{A_{nk}} (\theta - \theta_c)\,\mathrm{d}A, \tag{S11}$$

$$w_{3\,nk} = \frac{1}{A_k}\int_{A_{nk}} \cos\theta(\phi - \phi_c)\,\mathrm{d}A. \tag{M10}$$

The reference point (θ_c, ϕ_c), with implicitly including ρ_c component, is actually called the centroid in J99 (expressed as θ_n, ϕ_n). Note that Eqs. (S11) and (M10) are presented as intermediate formulations (Eqs. J99.9 and J99.10) during the derivation.

Before the final formulations of the remapping weights terms, an important characteristic is described here. It is reasonable to conclude that Eq. (M10) holds for any longitudinal origin; otherwise, the remapping weight $w_{3\,nk}$ would change its value according to the coordinate. Thus, in the computation of the weights for each source cell n, it would be safe to rotate around the pole by ϕ_{ofs}, which would simply correspond to replacing the longitudinal variable with a relative

one. Put formally, Eq. (M10) is reformulated into

$$\text{(M11)}\quad w_{3\,nk} = \frac{1}{A_k}\int_{A_{nk}} \cos\theta[(\phi-\phi_{\mathsf{ofs}})-(\phi_c-\phi_{\mathsf{ofs}})]\,\mathrm{d}A = \frac{1}{A_k}\int_{A_{nk}} \cos\theta[\tilde{\phi}-\tilde{\phi}_c]\,\mathrm{d}\tilde{A},$$

where $\tilde{\phi} = \phi - \phi_{\mathsf{ofs}}$. This is an identity for any ϕ_{ofs}. Equation (M11) is exactly the same formulation as Eq. (M10), thus it can be safely expressed using ϕ in terms of $\tilde{\phi}$ without ambiguities. The same replacement from ϕ to $\tilde{\phi}$ is performed on the other remapping weights.

J99 suggests to adopt the source grid cell center as ϕ_{ofs} for each source cell instead of the globally-fixed longitude origin. The numerical library Spherical Coordinate Remapping and Interpolation Package (SCRIP) does include this method. This suggestion is raised from the spherical coordinate system nature, where the longitude is multiple valued on one line on the sphere. Such problems can be easily avoided using this simple method.

Actually, the definition of central longitude is ambiguous for general shapes of the grid cell, which must be supplied by the user according to the source grid cell configuration. Since only the difference between the two relative longitudes adjusted by the offset longitude is used in the computation, the central value is of no particular significance. It is even possible to have the offset longitude fall outside the cell boundaries as far as it is enough to avoid the multiple-value longitude issues. This topic will be discussed later.

The final formulations of $w_{2\,nk}$ and $w_{3\,nk}$ conducted in the algorithm are obtained by expanding the reference point (θ_c, ϕ_c). Here, the reference point that corresponds to those defined in J99 is represented as (θ_n, ϕ_n). According to (J24), the position vectors in Eq. (M4) are transformed into the corresponding spherical coordinates with including the metric scale factor, as follows:

$$\text{(S12)}\qquad \theta_n = \frac{1}{A_n}\int_{A_n} \theta\ \mathrm{d}A,$$

$$\text{(S13)}\quad \phi_n\cos\theta = \frac{1}{A_n}\int_{A_n} \phi\cos\theta\ \mathrm{d}A.$$

Introducing these formulations of the reference coordinate into Eqs. (S11) and (M10), the final formulations of $w_{2\,nk}$ and $w_{3\,nk}$ are as follows:

$$\text{(S14)}\quad \underset{\mathsf{ORG}}{w_{2\,nk}} = \frac{1}{A_k}\int_{A_{nk}} \theta\ \mathrm{d}A - \frac{1}{A_k}\int_{A_{nk}} \mathrm{d}A\,\frac{1}{A_n}\int_{A_n}\theta\ \mathrm{d}A = \frac{1}{A_k}\int_{A_{nk}} \theta\ \mathrm{d}A - \frac{w_{1\,nk}}{A_n}\int_{A_n}\theta\ \mathrm{d}A,$$

$$\text{(M14)}\quad \underset{\mathsf{ORG}}{w_{3\,nk}} = \frac{1}{A_k}\int_{A_{nk}} \phi\cos\theta\ \mathrm{d}A - \frac{1}{A_k}\int_{A_{nk}} \mathrm{d}A\,\frac{1}{A_n}\int_{A_n}\phi\cos\theta\ \mathrm{d}A = \frac{1}{A_k}\int_{A_{nk}} \phi\cos\theta\ \mathrm{d}A - \frac{w_{1\,nk}}{A_n}\int_{A_n}\phi\cos\theta\ \mathrm{d}A,$$

which correspond to Eqs. (J99.9) and (J99.10), respectively. As explained above, Eq. (M14) is computed using $\tilde{\phi} = \phi - \phi_{\mathsf{ofs}}$ term, the longitude relative to a reference longitude ϕ_{ofs}:

$$\text{(M15)}\quad \underset{\mathsf{ORG}}{\tilde{w}_{3\,nk}} = \frac{1}{A_k}\int_{A_{nk}} \tilde{\phi}\cos\theta\ \mathrm{d}\tilde{A} - \frac{w_{1\,nk}}{A_n}\int_{A_n}\tilde{\phi}\cos\theta\ \mathrm{d}\tilde{A}.$$

The integral parts of the remapping coefficients $w_{1\,nk}$, $\underset{\mathsf{ORG}}{w_{2\,nk}}$ and $\underset{\mathsf{ORG}}{\tilde{w}_{3\,nk}}$ (Eqs. S10,S14 and M15) are computed by transforming it into a line integral using Gauss's divergent theorem (DK87, J99).

$$\text{(S15)}\quad \int_{A_{nk}} \mathrm{d}\tilde{A} = \oint_{C_{nk}} -\sin\theta\ \mathrm{d}\tilde{\phi},$$

$$\int_{A_{nk}} \theta \, \mathrm{d}\tilde{A} = \oint_{C_{nk}} -[\cos\theta + \theta \sin\theta] \, \mathrm{d}\tilde{\phi}, \tag{S16}$$

$$\int_{A_{nk}} \tilde{\phi} \cos\theta \, \mathrm{d}\tilde{A} = \oint_{C_{nk}} -\frac{\tilde{\phi}}{2}[\sin\theta\cos\theta + \theta] \, \mathrm{d}\tilde{\phi}, \tag{S17}$$

respectively, where C_{nk} is the counterclockwise path around the region A_{nk}.

Based on the author's exploration of the SCRIP source code and the Climate Data Operators (CDO) source code, the formulations correspond to Eqs. (S14) and (M15) being implemented.

S2 Supplementary figures

In the main paper, mostly the results of experiment A2 are shown and discussed. This supplement includes those of the other two experiments, A1 and A3. Although the results of A2 is presented in the main paper, they are repeated in this supplement for easy comparison.

Figures S1 to S24 are the result of one-time remapping for all the experiment (A1, A2, A3, schemes N and P, four variations of the destination grids).

Tables S1, S2, S3 and S4 are summary of the metrics $|L_g|$, $\|E\|_{L_2}$, $\|E\|_{L_\infty}$ and $\|E\|_{H_1}$, respectively for one-time forward remapping.

Tables S5, S6, S7 and S8 are summary of the metrics $|L_g|$, $\|E\|_{L_2}$, $\|E\|_{L_\infty}$ and $\|E\|_{H_1}$, respectively for the fields after 1000-time iterative remapping.

The tables follow those in the main paper. the second column indicates the offset longitude, where mid, edge, global correspond to the $\phi_{\mathsf{ofs}} = (\phi_0 + \phi_1)/2$, $\phi_{\mathsf{ofs}} = \phi_1$, and $\phi_{\mathsf{ofs}} = 180^\circ$ cases, respectively. Destination grid sizes are $(N_\theta, N_\phi) = (90, 180)$, $(180, 360)$, $(360, 720)$, $(720, 1440)$. The digits which are different from corresponding mid-cell experiments are written in bold. When the first different digit comes after 7 from the decimal point, it is written as $(n \; d)$ where n denotes the largest order to show difference. Also, computation for some cases stops before 1000 iteration, which is denoted as ∞ in the tables.

Figures S25 and S26 are the evolution of the metrics for experiment A1 and A3, respectively, which show $\|E\|_{L_2}$, $\|E\|_{L_\infty}$ and $\|E\|_{H_1}$ through 1000-times iterative remapping.

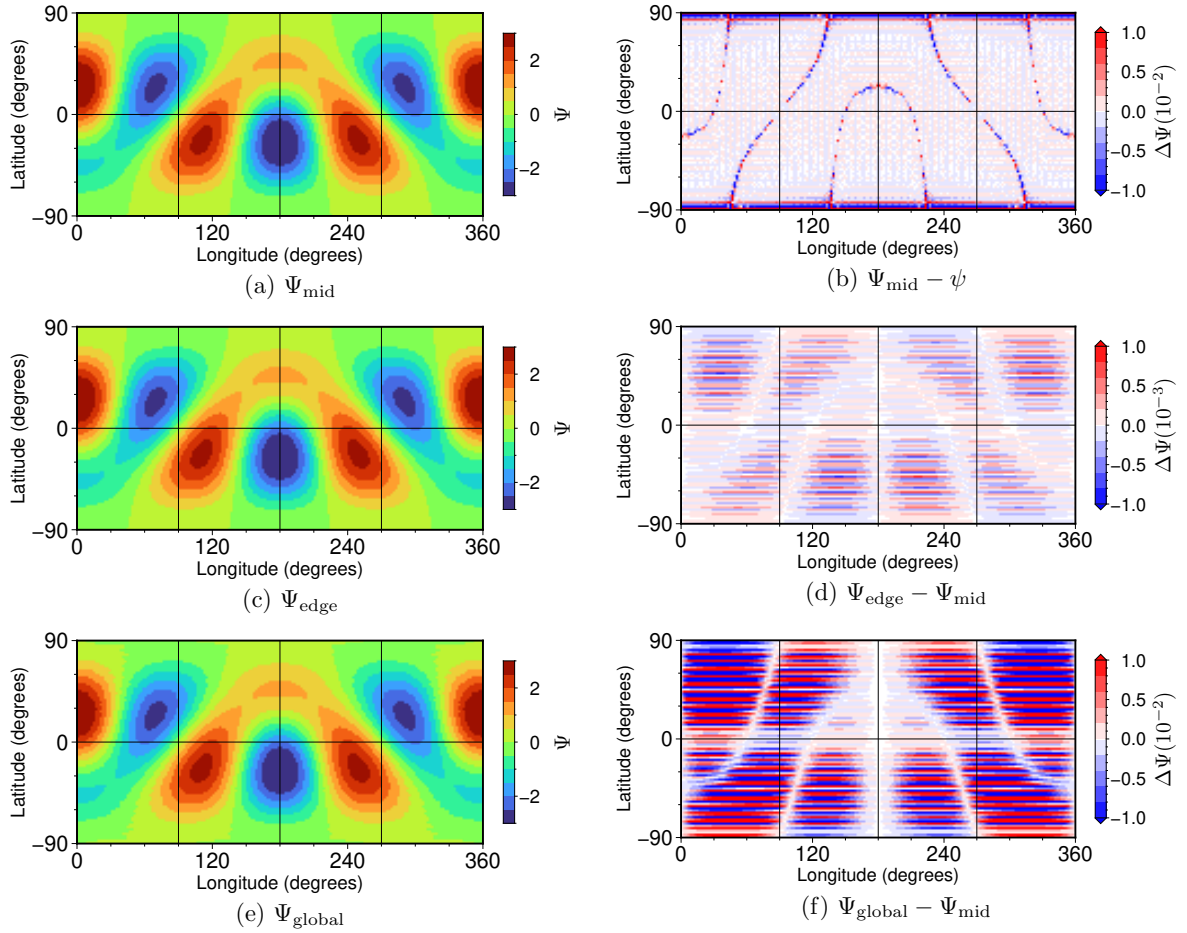

(a) Ψ_{mid} (b) $\Psi_{\mathrm{mid}} - \psi$

(c) Ψ_{edge} (d) $\Psi_{\mathrm{edge}} - \Psi_{\mathrm{mid}}$

(e) Ψ_{global} (f) $\Psi_{\mathrm{global}} - \Psi_{\mathrm{mid}}$

Figure S1: Results of sensitivity experiments A1 using scheme N for the offset longitudes where mid, edge, global correspond to the $\phi_{\mathsf{ofs}} = (\phi_0 + \phi_1)/2$, $\phi_{\mathsf{ofs}} = \phi_1$, and $\phi_{\mathsf{ofs}} = 180°$ cases, respectively. (a) One-time remapped field for mid-offset case (Ψ_{mid}). (b) Error in the remapped field of the mid-offset case ($\Psi_{\mathrm{mid}} - \psi$). (c) One-time remapped field for edge-offset case (Ψ_{edge}). (d) Difference between edge- and mid-offset cases ($\Psi_{\mathrm{edge}} - \Psi_{\mathrm{mid}}$). (e) Remapped field field for global-offset case (Ψ_{global}). (f) Difference between global- and mid-offset cases ($\Psi_{\mathrm{global}} - \Psi_{\mathrm{mid}}$). Resolution of the destination grid cells is $(N_\theta, N_\phi) = (90, 180)$.

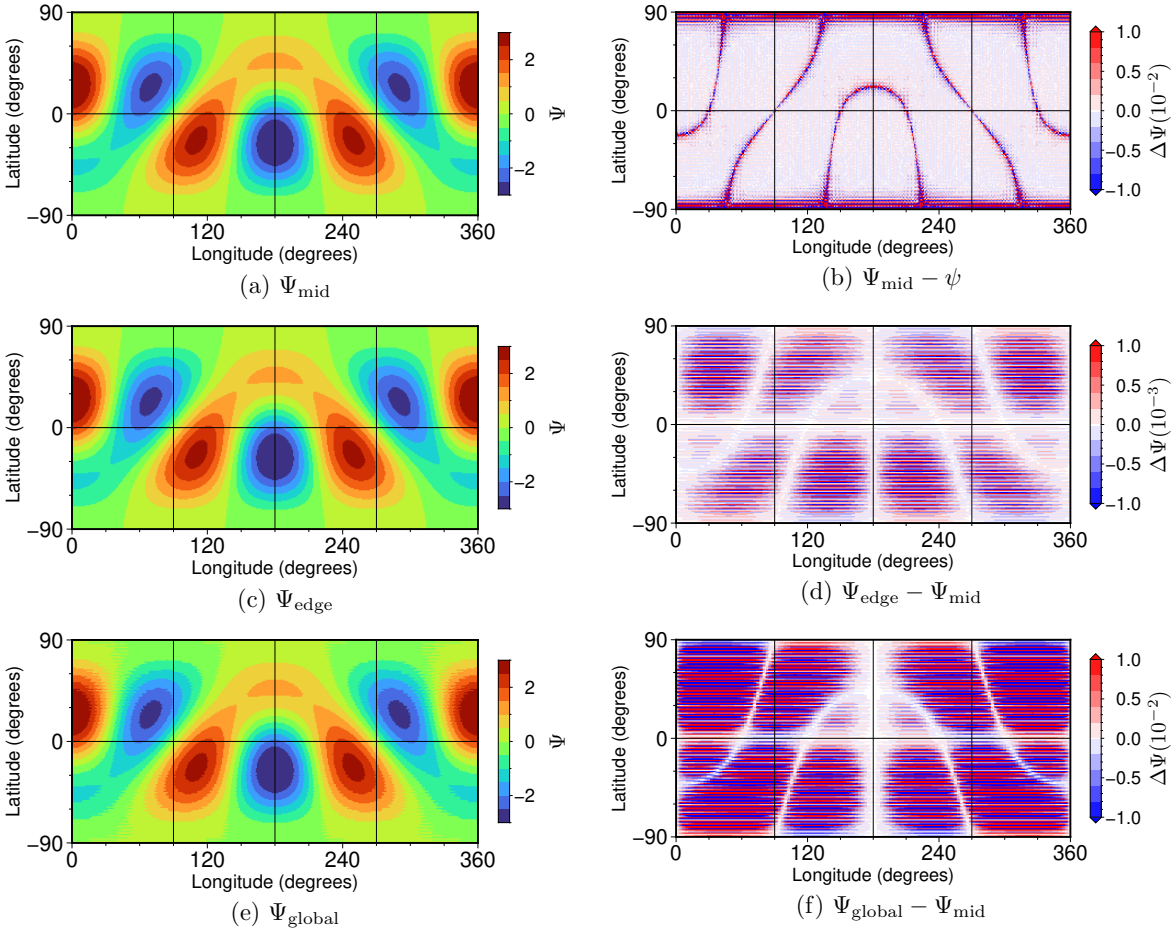

(a) Ψ_{mid} (b) $\Psi_{\mathrm{mid}} - \psi$

(c) Ψ_{edge} (d) $\Psi_{\mathrm{edge}} - \Psi_{\mathrm{mid}}$

(e) Ψ_{global} (f) $\Psi_{\mathrm{global}} - \Psi_{\mathrm{mid}}$

Figure S2: The same as Fig. (S1) but resolution of the destination grid cells is $(N_\theta, N_\phi) = (180, 360)$.

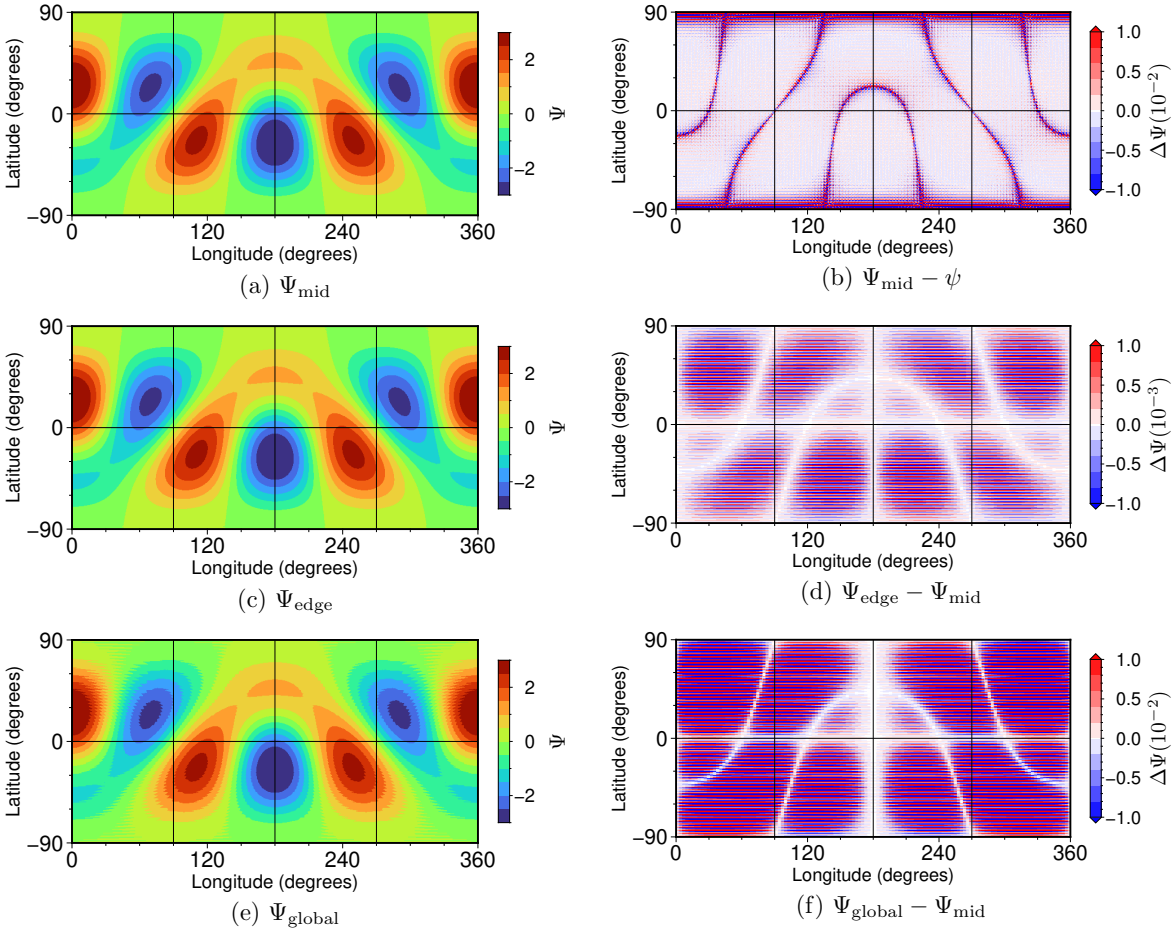

(a) Ψ_{mid} (b) $\Psi_{\mathrm{mid}} - \psi$

(c) Ψ_{edge} (d) $\Psi_{\mathrm{edge}} - \Psi_{\mathrm{mid}}$

(e) Ψ_{global} (f) $\Psi_{\mathrm{global}} - \Psi_{\mathrm{mid}}$

Figure S3: The same as Fig. (S1) but resolution of the destination grid cells is $(N_\theta, N_\phi) = (360, 720)$.

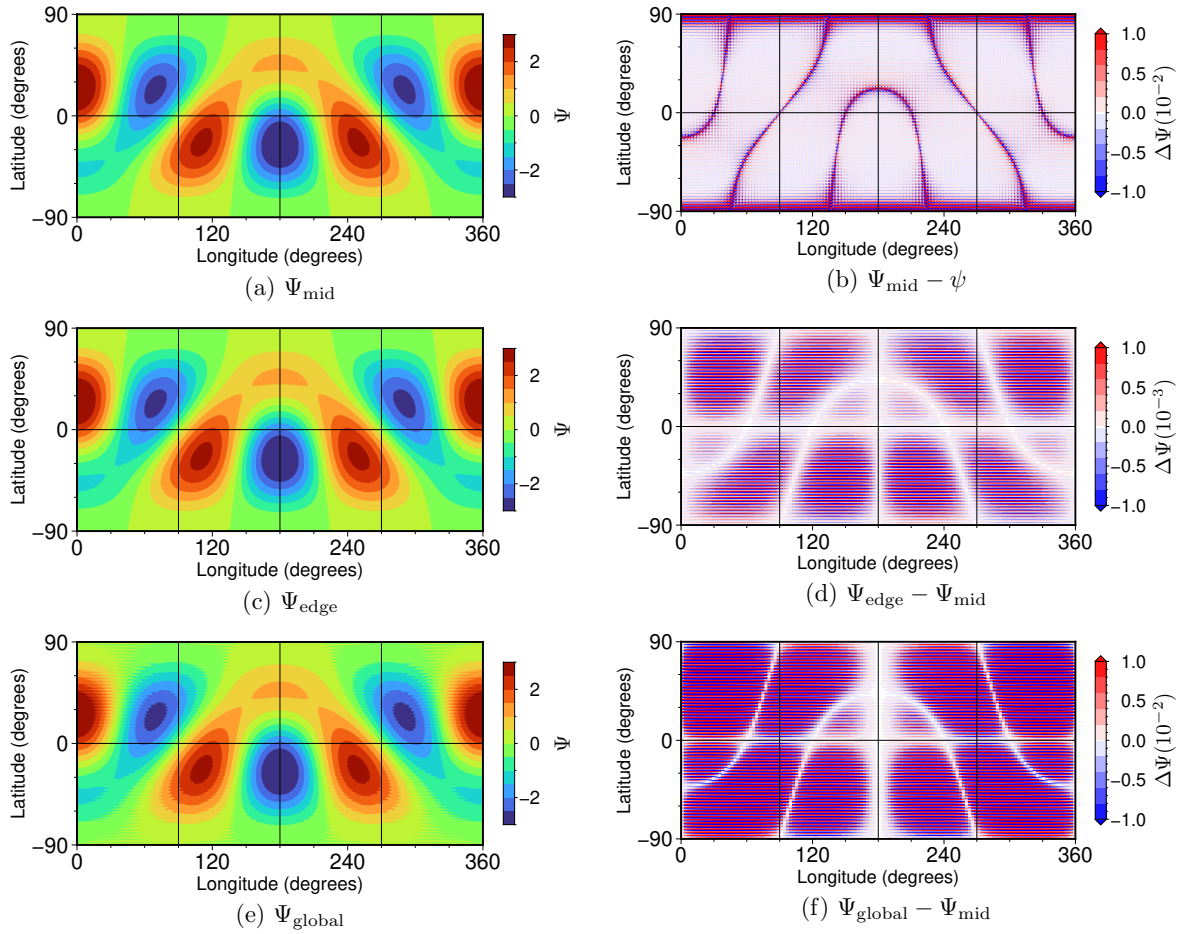

(a) Ψ_{mid} (b) $\Psi_{\mathrm{mid}} - \psi$

(c) Ψ_{edge} (d) $\Psi_{\mathrm{edge}} - \Psi_{\mathrm{mid}}$

(e) Ψ_{global} (f) $\Psi_{\mathrm{global}} - \Psi_{\mathrm{mid}}$

Figure S4: The same as Fig. (S1) but resolution of the destination grid cells is $(N_\theta, N_\phi) = (720, 1440)$.

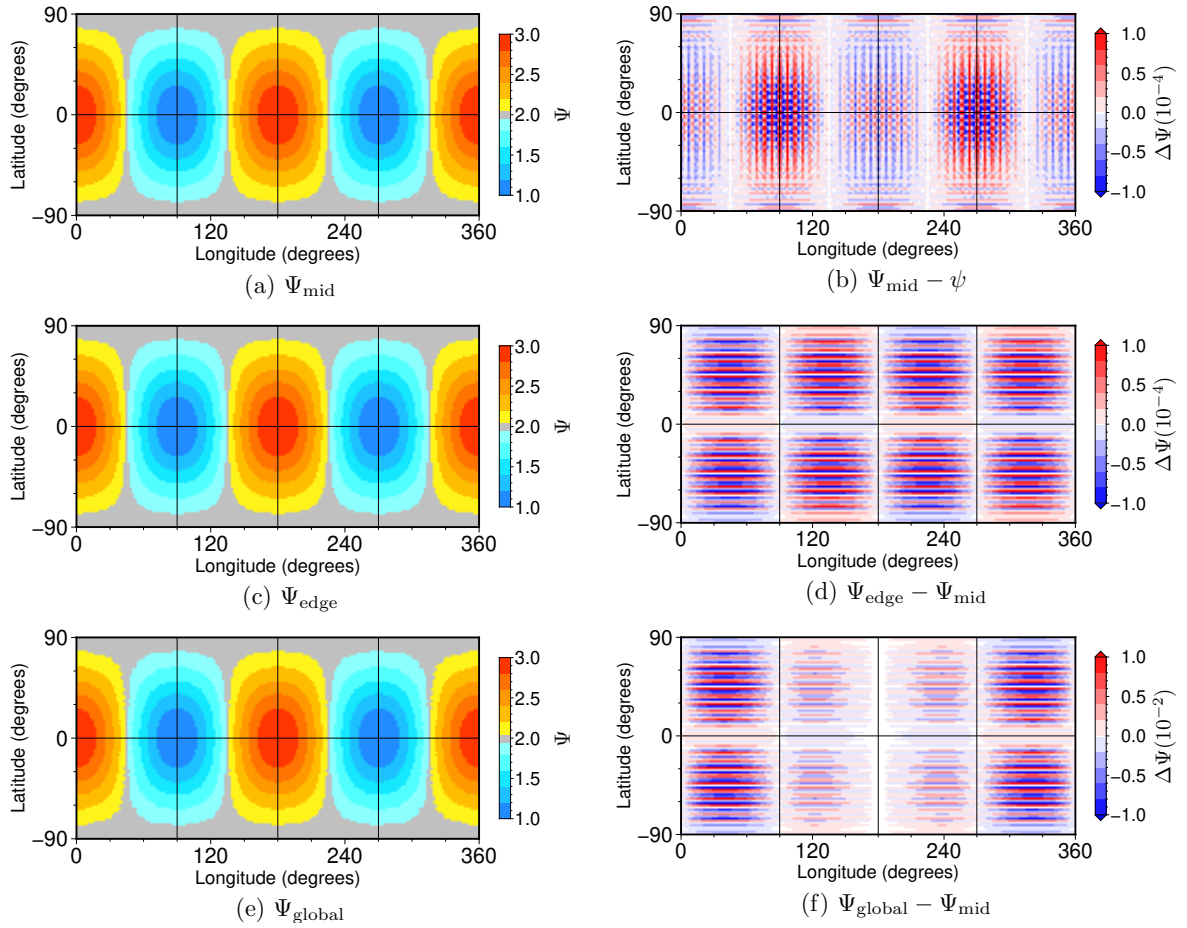

(a) Ψ_{mid} (b) $\Psi_{\mathrm{mid}} - \psi$

(c) Ψ_{edge} (d) $\Psi_{\mathrm{edge}} - \Psi_{\mathrm{mid}}$

(e) Ψ_{global} (f) $\Psi_{\mathrm{global}} - \Psi_{\mathrm{mid}}$

Figure S5: Results of sensitivity experiments A2 using scheme N for the offset longitudes where mid, edge, global correspond to the $\phi_{\mathsf{ofs}} = (\phi_0 + \phi_1)/2$, $\phi_{\mathsf{ofs}} = \phi_1$, and $\phi_{\mathsf{ofs}} = 180^\circ$ cases, respectively. (a) One-time remapped field for mid-offset case (Ψ_{mid}). (b) Error in the remapped field of the mid-offset case ($\Psi_{\mathrm{mid}} - \psi$). (c) One-time remapped field for edge-offset case (Ψ_{edge}). (d) Difference between edge- and mid-offset cases ($\Psi_{\mathrm{edge}} - \Psi_{\mathrm{mid}}$). (e) Remapped field field for global-offset case (Ψ_{global}). (f) Difference between global- and mid-offset cases ($\Psi_{\mathrm{global}} - \Psi_{\mathrm{mid}}$). Resolution of the destination grid cells is $(N_\theta, N_\phi) = (90, 180)$.

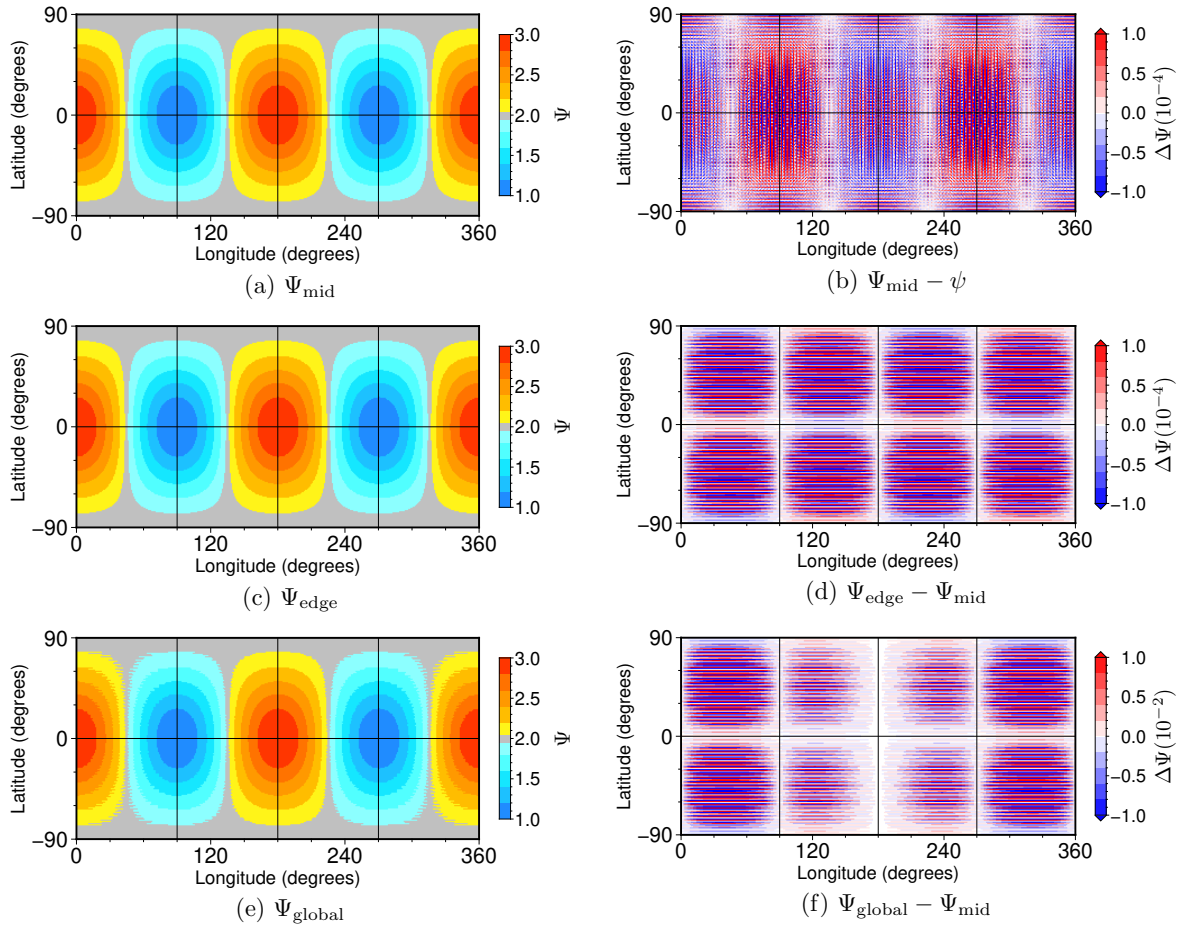

(a) Ψ_{mid} (b) $\Psi_{\mathrm{mid}} - \psi$

(c) Ψ_{edge} (d) $\Psi_{\mathrm{edge}} - \Psi_{\mathrm{mid}}$

(e) Ψ_{global} (f) $\Psi_{\mathrm{global}} - \Psi_{\mathrm{mid}}$

Figure S6: The same as Fig. (S5) but resolution of the destination grid cells is $(N_\theta, N_\phi) = (180, 360)$.

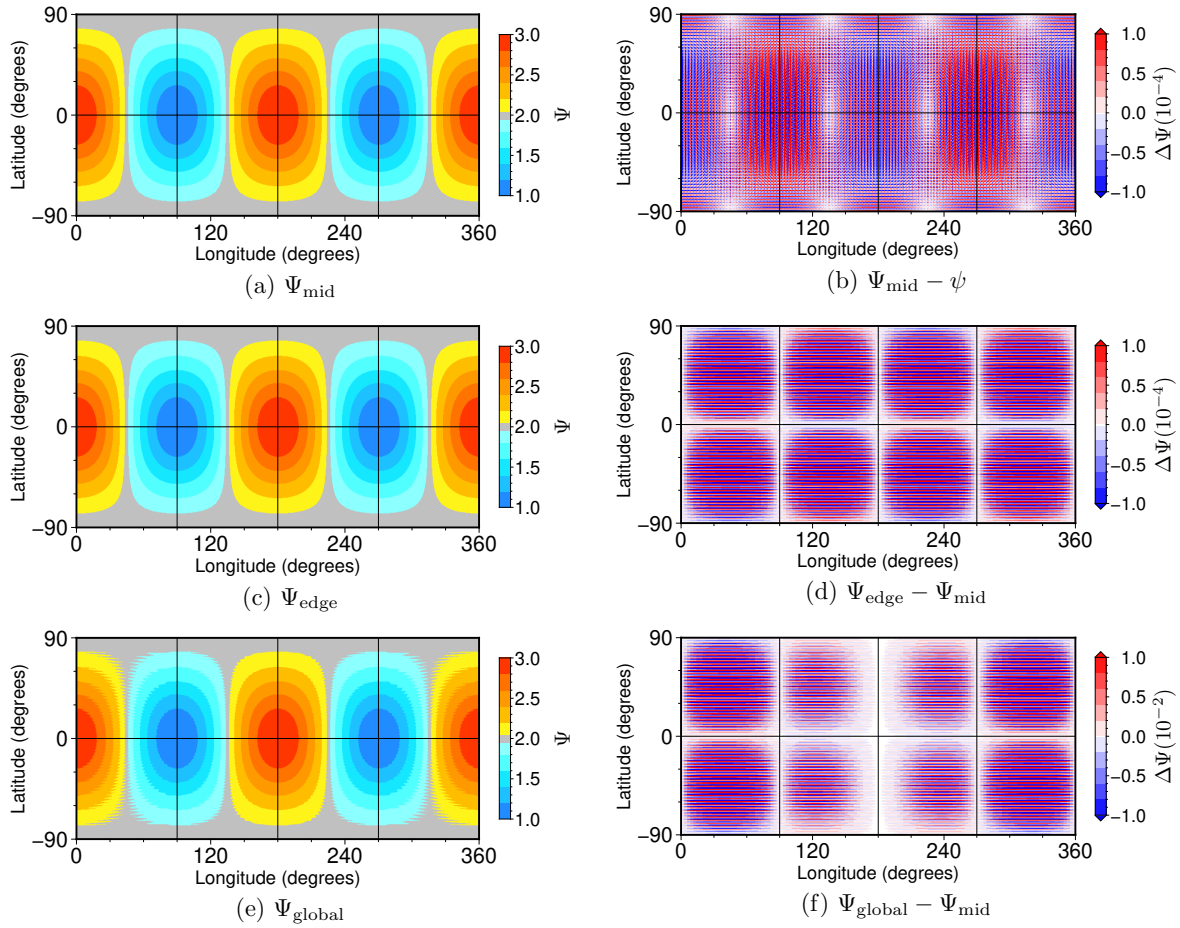

(a) Ψ_{mid} (b) $\Psi_{\mathrm{mid}} - \psi$

(c) Ψ_{edge} (d) $\Psi_{\mathrm{edge}} - \Psi_{\mathrm{mid}}$

(e) Ψ_{global} (f) $\Psi_{\mathrm{global}} - \Psi_{\mathrm{mid}}$

Figure S7: The same as Fig. (S5) but resolution of the destination grid cells is $(N_\theta, N_\phi) = (360, 720)$.

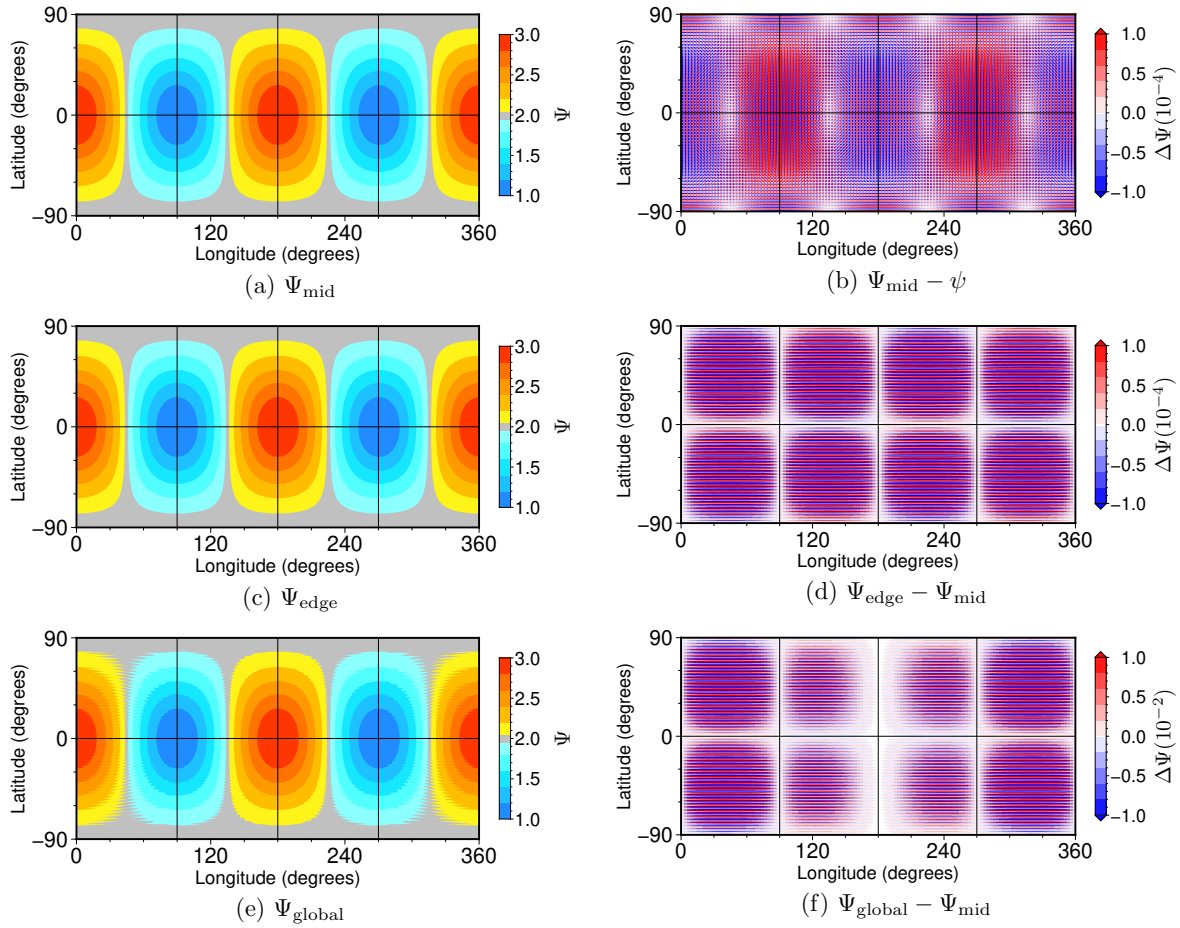

(a) $\Psi_{\rm mid}$ (b) $\Psi_{\rm mid} - \psi$

(c) $\Psi_{\rm edge}$ (d) $\Psi_{\rm edge} - \Psi_{\rm mid}$

(e) $\Psi_{\rm global}$ (f) $\Psi_{\rm global} - \Psi_{\rm mid}$

Figure S8: The same as Fig. (S5) but resolution of the destination grid cells is $(N_\theta, N_\phi) = (720, 1440)$.

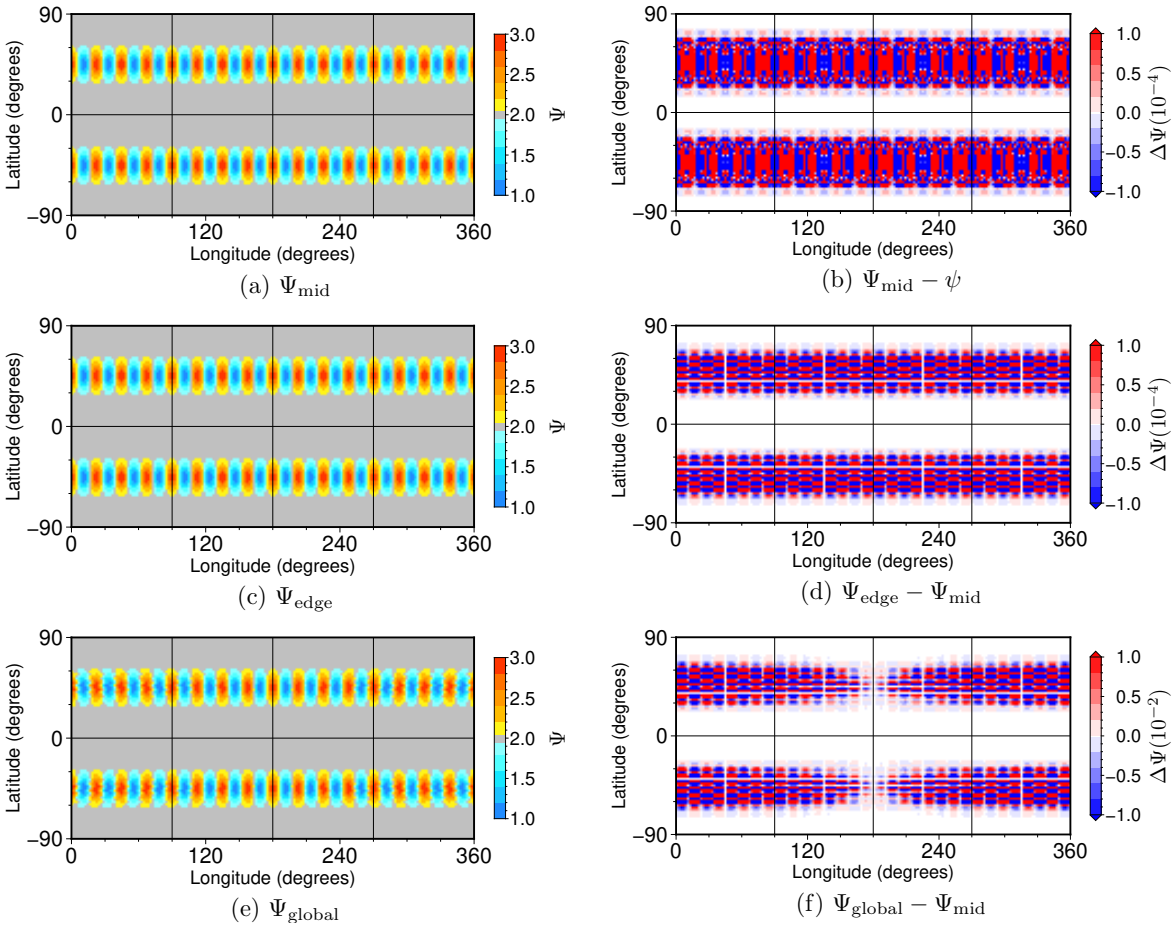

(a) Ψ_{mid} (b) $\Psi_{\mathrm{mid}} - \psi$

(c) Ψ_{edge} (d) $\Psi_{\mathrm{edge}} - \Psi_{\mathrm{mid}}$

(e) Ψ_{global} (f) $\Psi_{\mathrm{global}} - \Psi_{\mathrm{mid}}$

Figure S9: Results of sensitivity experiments A3 using scheme N for the offset longitudes where mid, edge, global correspond to the $\phi_{\mathsf{ofs}} = (\phi_0 + \phi_1)/2$, $\phi_{\mathsf{ofs}} = \phi_1$, and $\phi_{\mathsf{ofs}} = 180^\circ$ cases, respectively. (a) One-time remapped field for mid-offset case (Ψ_{mid}). (b) Error in the remapped field of the mid-offset case ($\Psi_{\mathrm{mid}} - \psi$). (c) One-time remapped field for edge-offset case (Ψ_{edge}). (d) Difference between edge- and mid-offset cases ($\Psi_{\mathrm{edge}} - \Psi_{\mathrm{mid}}$). (e) Remapped field field for global-offset case (Ψ_{global}). (f) Difference between global- and mid-offset cases ($\Psi_{\mathrm{global}} - \Psi_{\mathrm{mid}}$). Resolution of the destination grid cells is $(N_\theta, N_\phi) = (90, 180)$.

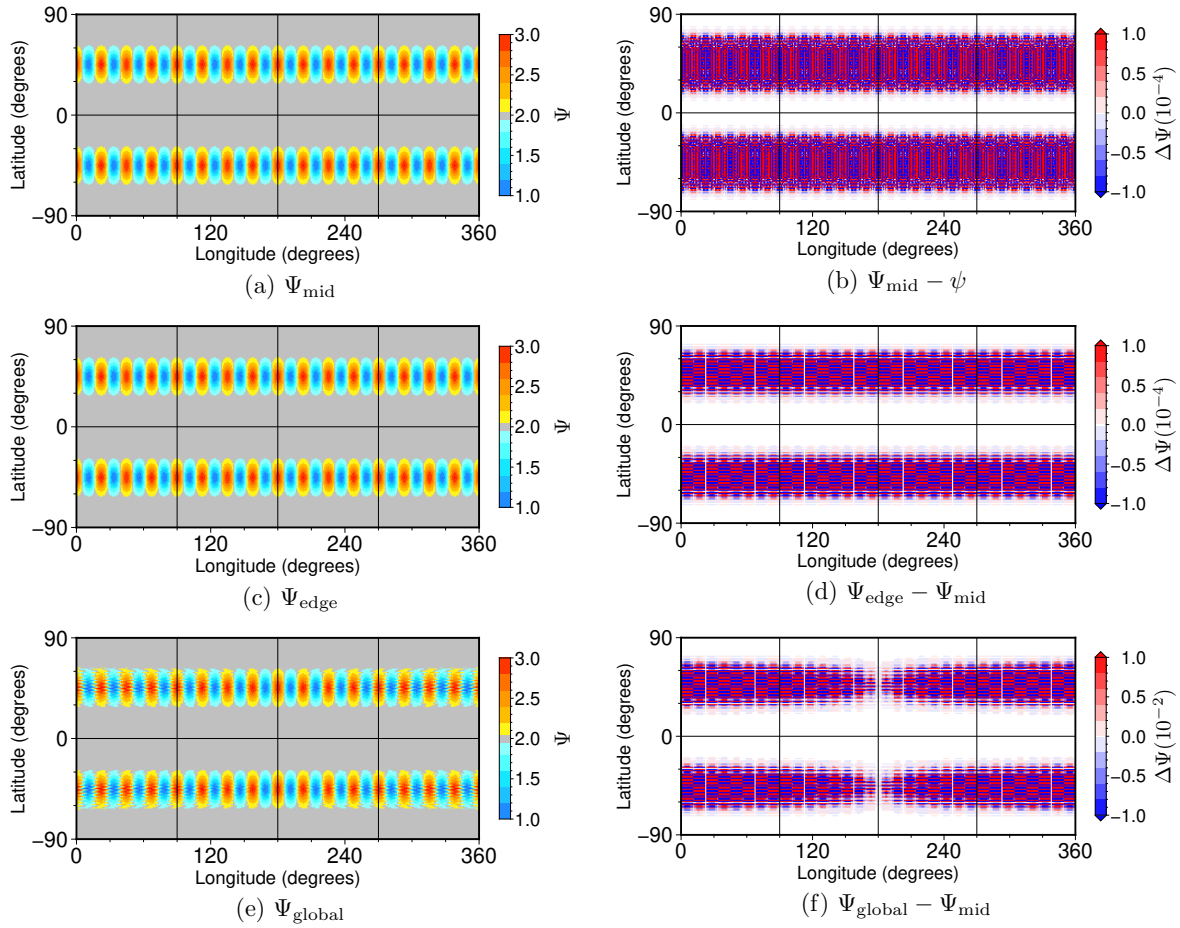

(a) $\Psi_{\rm mid}$ (b) $\Psi_{\rm mid} - \psi$

(c) $\Psi_{\rm edge}$ (d) $\Psi_{\rm edge} - \Psi_{\rm mid}$

(e) $\Psi_{\rm global}$ (f) $\Psi_{\rm global} - \Psi_{\rm mid}$

Figure S10: The same as Fig. (S9) but resolution of the destination grid cells is $(N_\theta, N_\phi) = (180, 360)$.

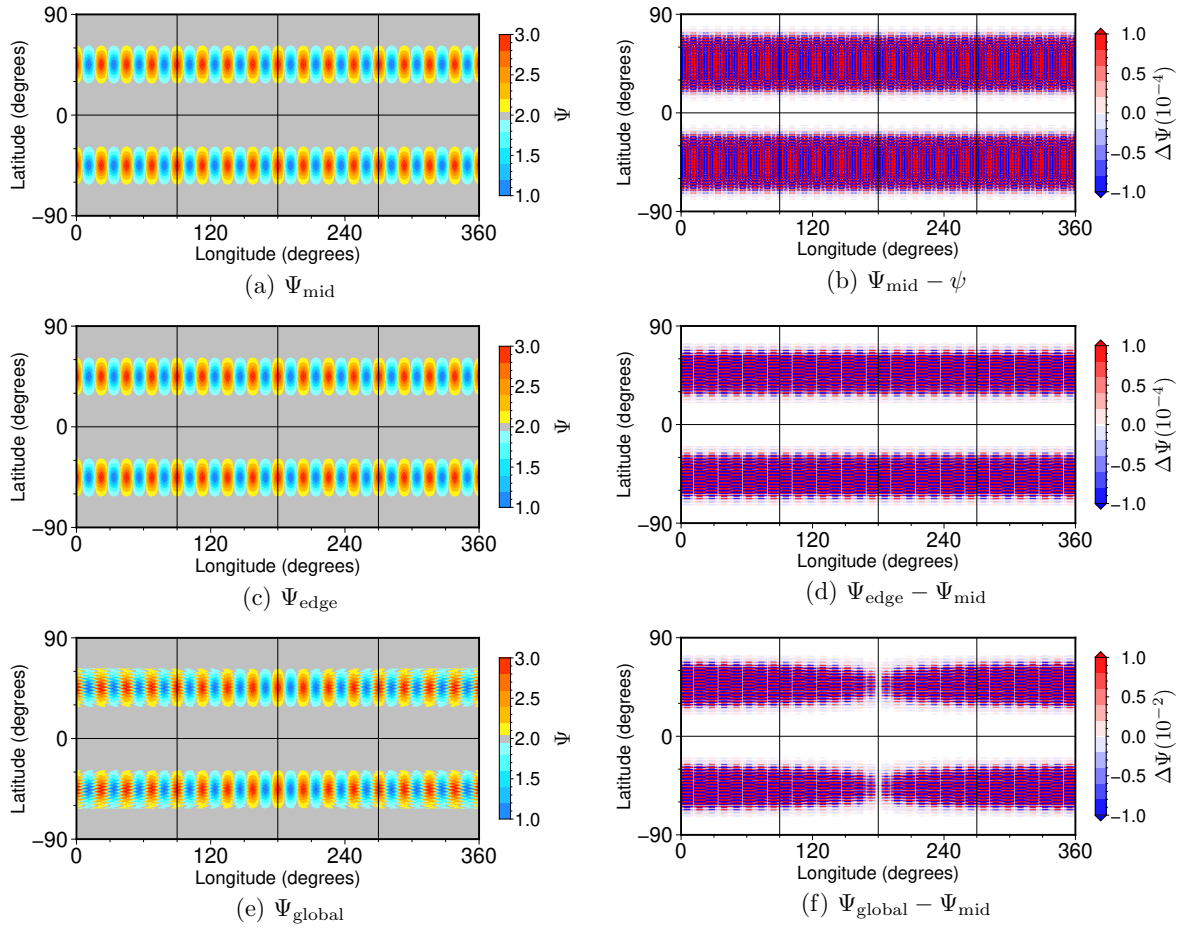

(a) Ψ_{mid} (b) $\Psi_{\mathrm{mid}} - \psi$

(c) Ψ_{edge} (d) $\Psi_{\mathrm{edge}} - \Psi_{\mathrm{mid}}$

(e) Ψ_{global} (f) $\Psi_{\mathrm{global}} - \Psi_{\mathrm{mid}}$

Figure S11: The same as Fig. (S9) but resolution of the destination grid cells is $(N_\theta, N_\phi) = (360, 720)$.

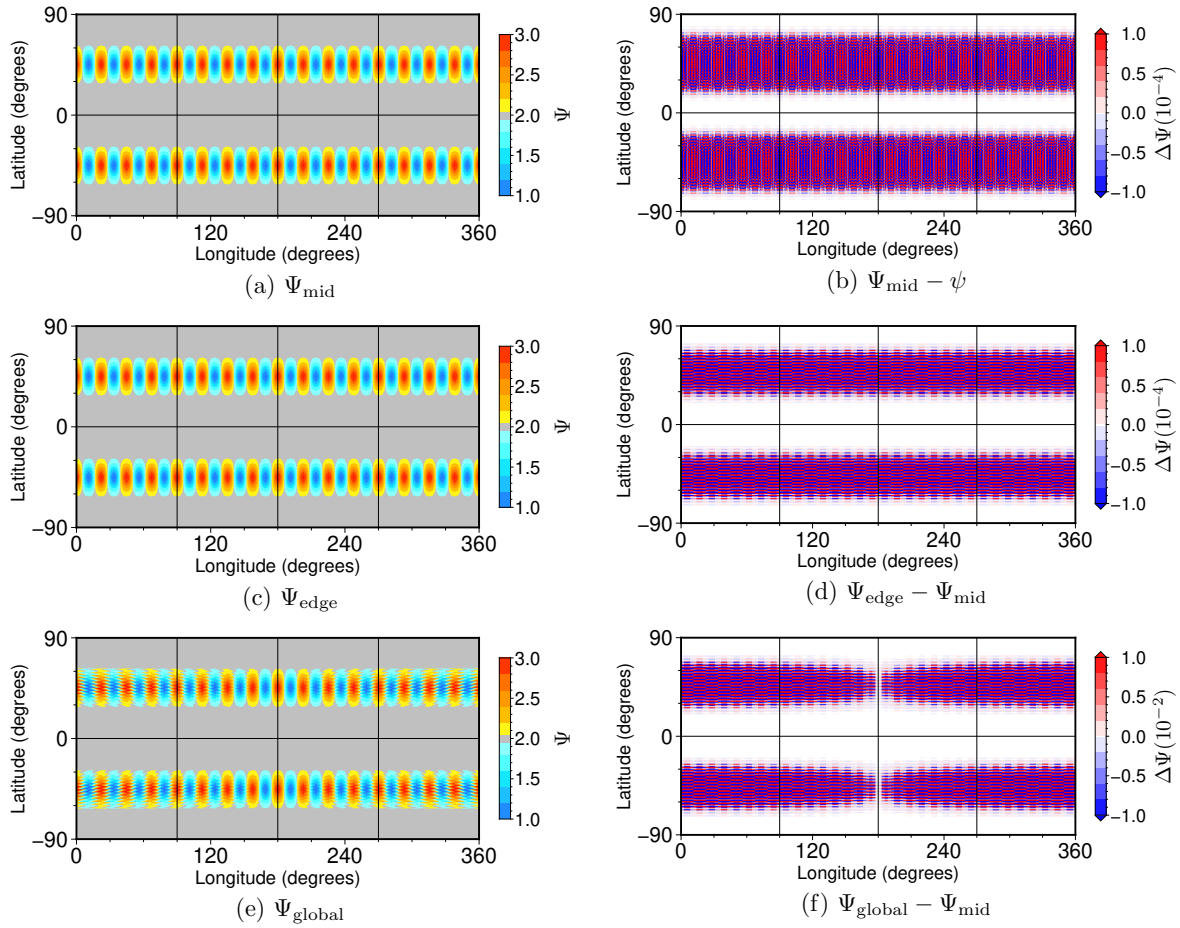

(a) Ψ_{mid} (b) $\Psi_{\mathrm{mid}} - \psi$

(c) Ψ_{edge} (d) $\Psi_{\mathrm{edge}} - \Psi_{\mathrm{mid}}$

(e) Ψ_{global} (f) $\Psi_{\mathrm{global}} - \Psi_{\mathrm{mid}}$

Figure S12: The same as Fig. (S9) but resolution of the destination grid cells is $(N_\theta, N_\phi) = (720, 1440)$.

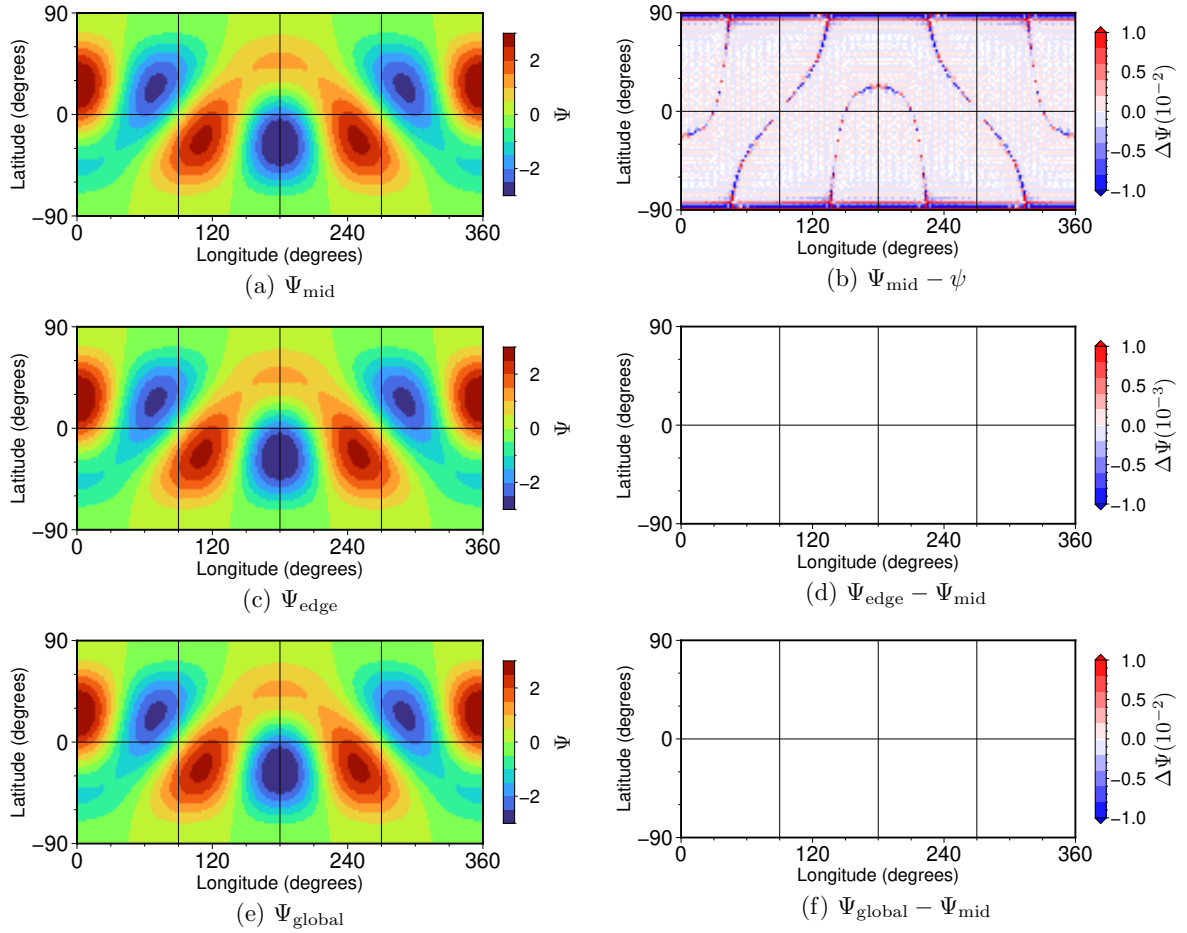

(a) Ψ_{mid} (b) $\Psi_{\mathrm{mid}} - \psi$

(c) Ψ_{edge} (d) $\Psi_{\mathrm{edge}} - \Psi_{\mathrm{mid}}$

(e) Ψ_{global} (f) $\Psi_{\mathrm{global}} - \Psi_{\mathrm{mid}}$

Figure S13: Results of sensitivity experiments A1 using Schemes P for the offset longitudes where mid, edge, global correspond to the $\phi_{\mathsf{ofs}} = (\phi_0 + \phi_1)/2$, $\phi_{\mathsf{ofs}} = \phi_1$, and $\phi_{\mathsf{ofs}} = 180°$ cases, respectively. (a) One-time remapped field for mid-offset case (Ψ_{mid}). (b) Error in the remapped field of the mid-offset case ($\Psi_{\mathrm{mid}} - \psi$). (c) One-time remapped field for edge-offset case (Ψ_{edge}). (d) Difference between edge- and mid-offset cases ($\Psi_{\mathrm{edge}} - \Psi_{\mathrm{mid}}$). (e) Remapped field field for global-offset case (Ψ_{global}). (f) Difference between global- and mid-offset cases ($\Psi_{\mathrm{global}} - \Psi_{\mathrm{mid}}$). Resolution of the destination grid cells is $(N_\theta, N_\phi) = (90, 180)$.

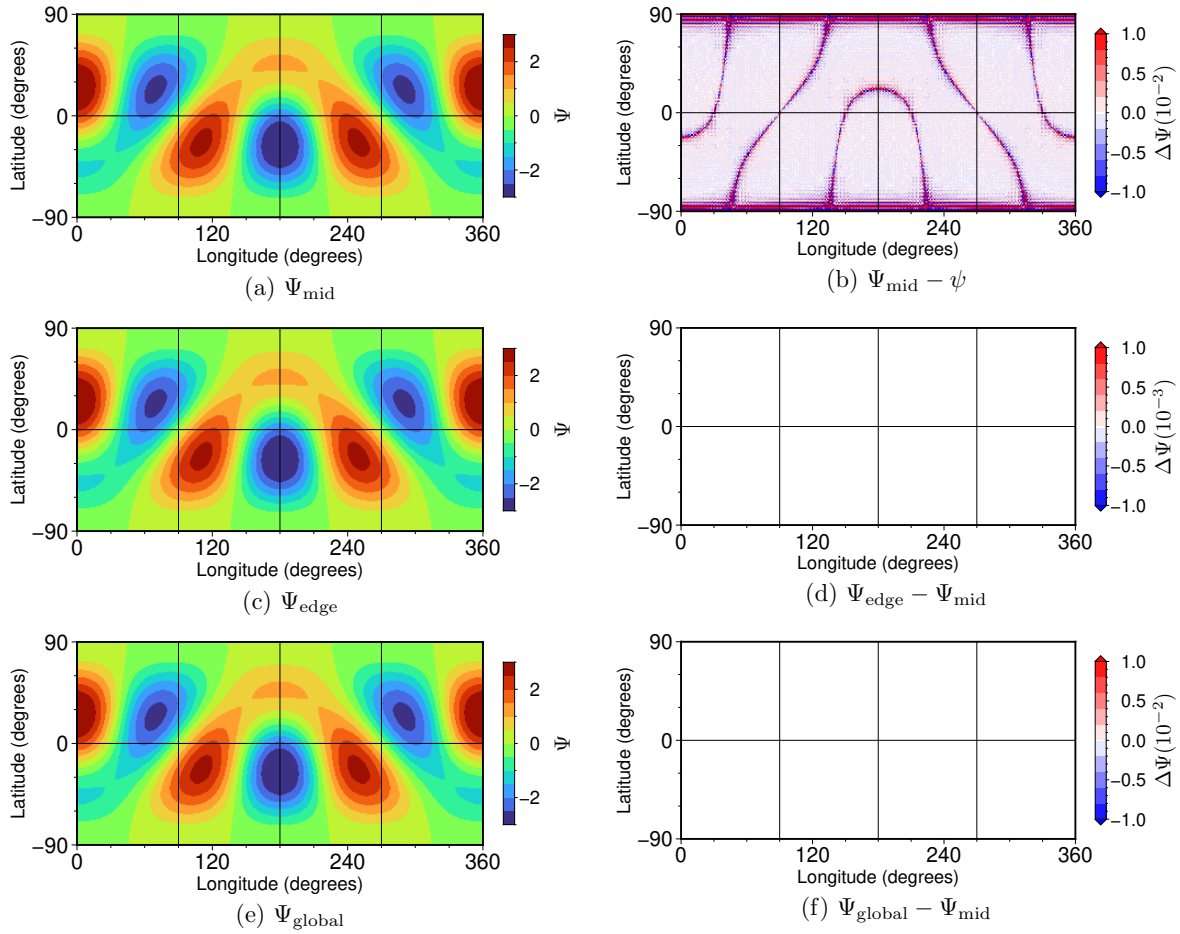

(a) Ψ_{mid} (b) $\Psi_{\mathrm{mid}} - \psi$

(c) Ψ_{edge} (d) $\Psi_{\mathrm{edge}} - \Psi_{\mathrm{mid}}$

(e) Ψ_{global} (f) $\Psi_{\mathrm{global}} - \Psi_{\mathrm{mid}}$

Figure S14: The same as Fig. (S13) but resolution of the destination grid cells is $(N_\theta, N_\phi) = (180, 360)$.

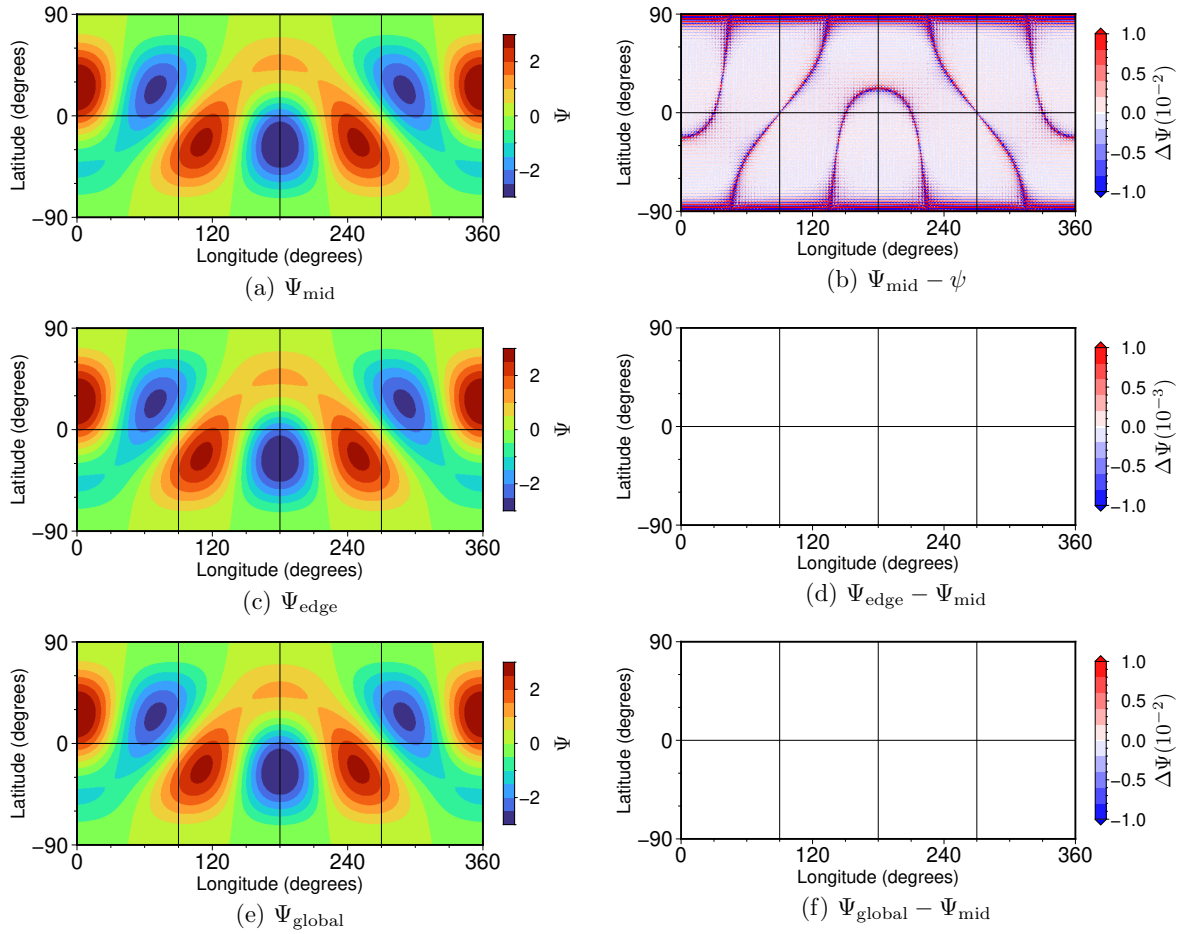

(a) Ψ_{mid} (b) $\Psi_{\mathrm{mid}} - \psi$

(c) Ψ_{edge} (d) $\Psi_{\mathrm{edge}} - \Psi_{\mathrm{mid}}$

(e) Ψ_{global} (f) $\Psi_{\mathrm{global}} - \Psi_{\mathrm{mid}}$

Figure S15: The same as Fig. (S13) but resolution of the destination grid cells is $(N_\theta, N_\phi) = (360, 720)$.

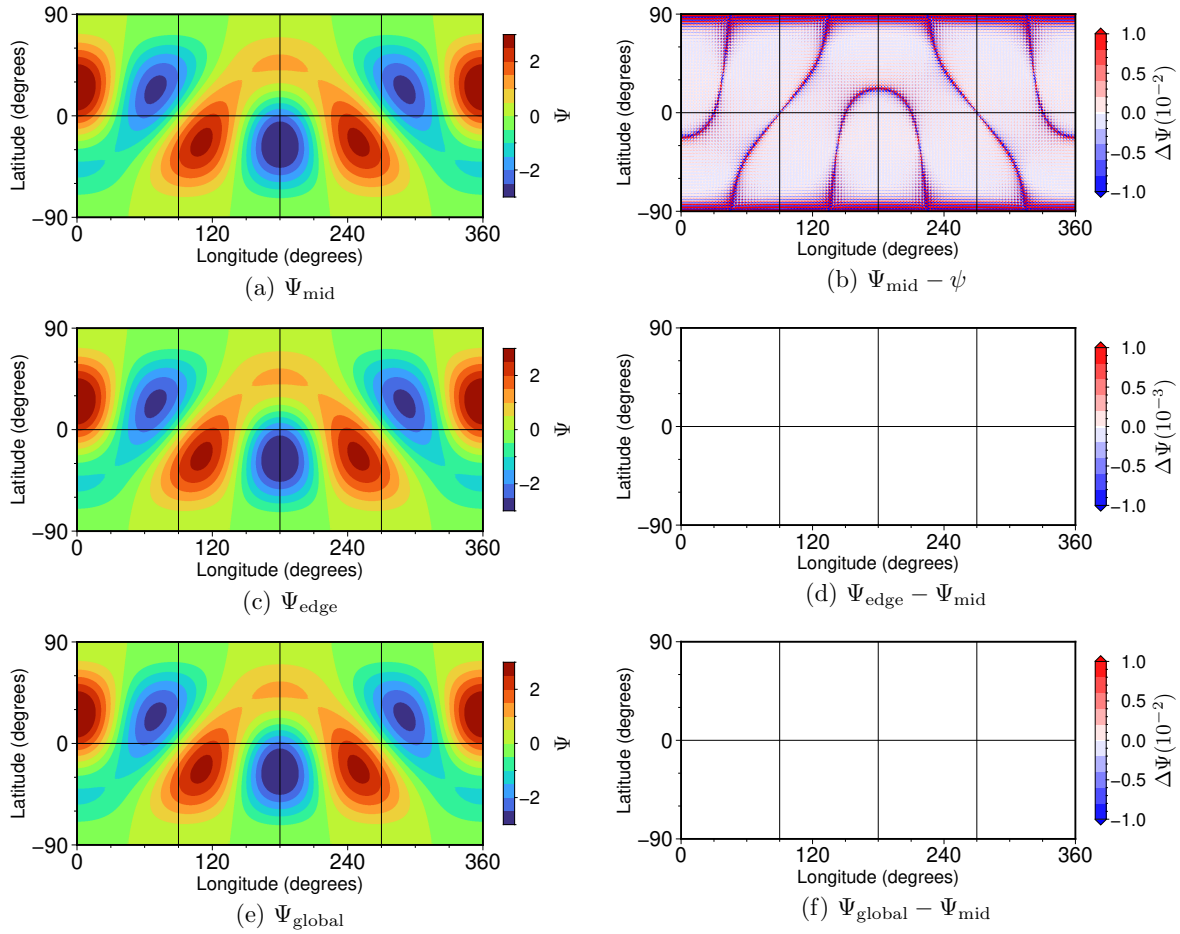

(a) Ψ_{mid} (b) $\Psi_{\mathrm{mid}} - \psi$

(c) Ψ_{edge} (d) $\Psi_{\mathrm{edge}} - \Psi_{\mathrm{mid}}$

(e) Ψ_{global} (f) $\Psi_{\mathrm{global}} - \Psi_{\mathrm{mid}}$

Figure S16: The same as Fig. (S13) but resolution of the destination grid cells is $(N_\theta, N_\phi) = (720, 1440)$.

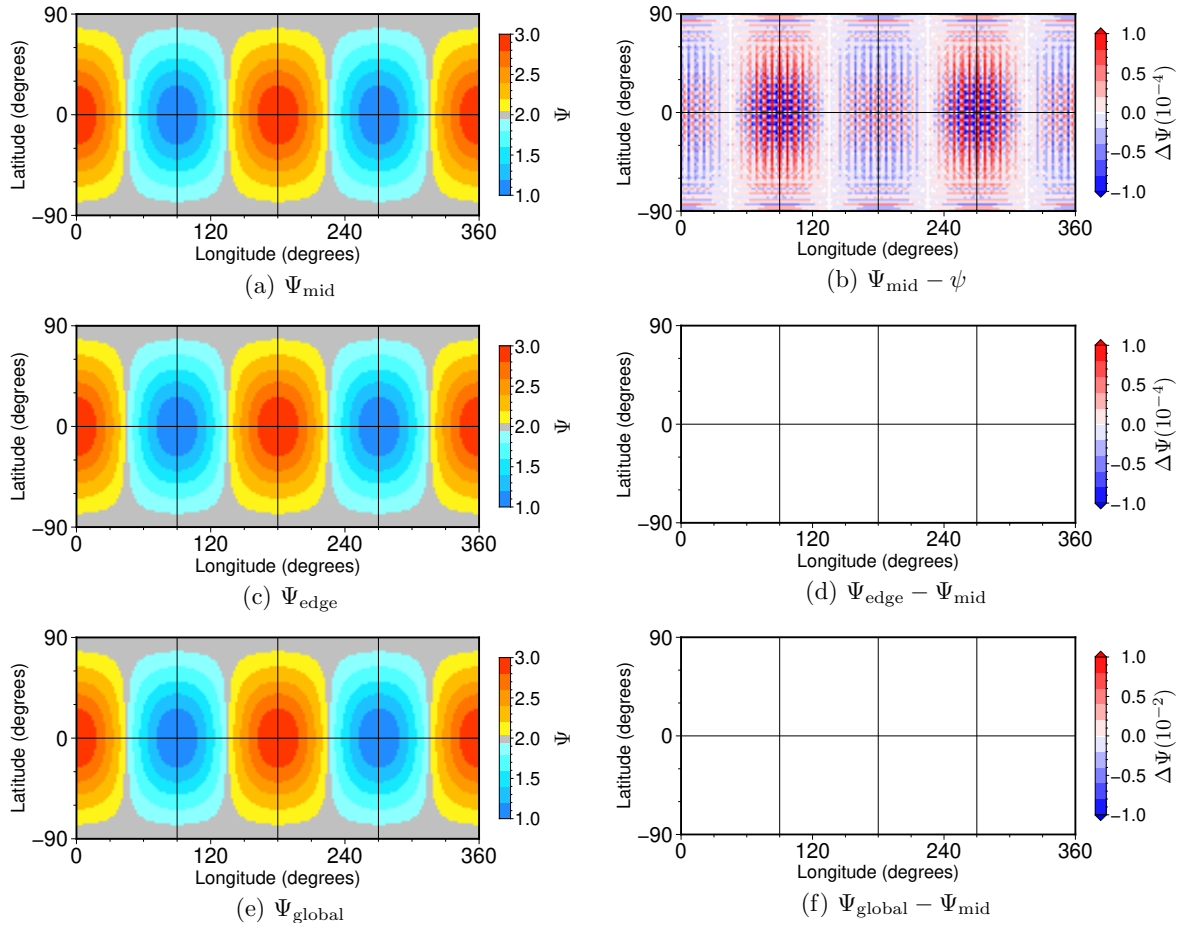

(a) Ψ_{mid} (b) $\Psi_{\mathrm{mid}} - \psi$

(c) Ψ_{edge} (d) $\Psi_{\mathrm{edge}} - \Psi_{\mathrm{mid}}$

(e) Ψ_{global} (f) $\Psi_{\mathrm{global}} - \Psi_{\mathrm{mid}}$

Figure S17: Results of sensitivity experiments A2 using Schemes P for the offset longitudes where mid, edge, global correspond to the $\phi_{\mathsf{ofs}} = (\phi_0 + \phi_1)/2$, $\phi_{\mathsf{ofs}} = \phi_1$, and $\phi_{\mathsf{ofs}} = 180^\circ$ cases, respectively. (a) One-time remapped field for mid-offset case (Ψ_{mid}). (b) Error in the remapped field of the mid-offset case ($\Psi_{\mathrm{mid}} - \psi$). (c) One-time remapped field for edge-offset case (Ψ_{edge}). (d) Difference between edge- and mid-offset cases ($\Psi_{\mathrm{edge}} - \Psi_{\mathrm{mid}}$). (e) Remapped field field for global-offset case (Ψ_{global}). (f) Difference between global- and mid-offset cases ($\Psi_{\mathrm{global}} - \Psi_{\mathrm{mid}}$). Resolution of the destination grid cells is $(N_\theta, N_\phi) = (90, 180)$.

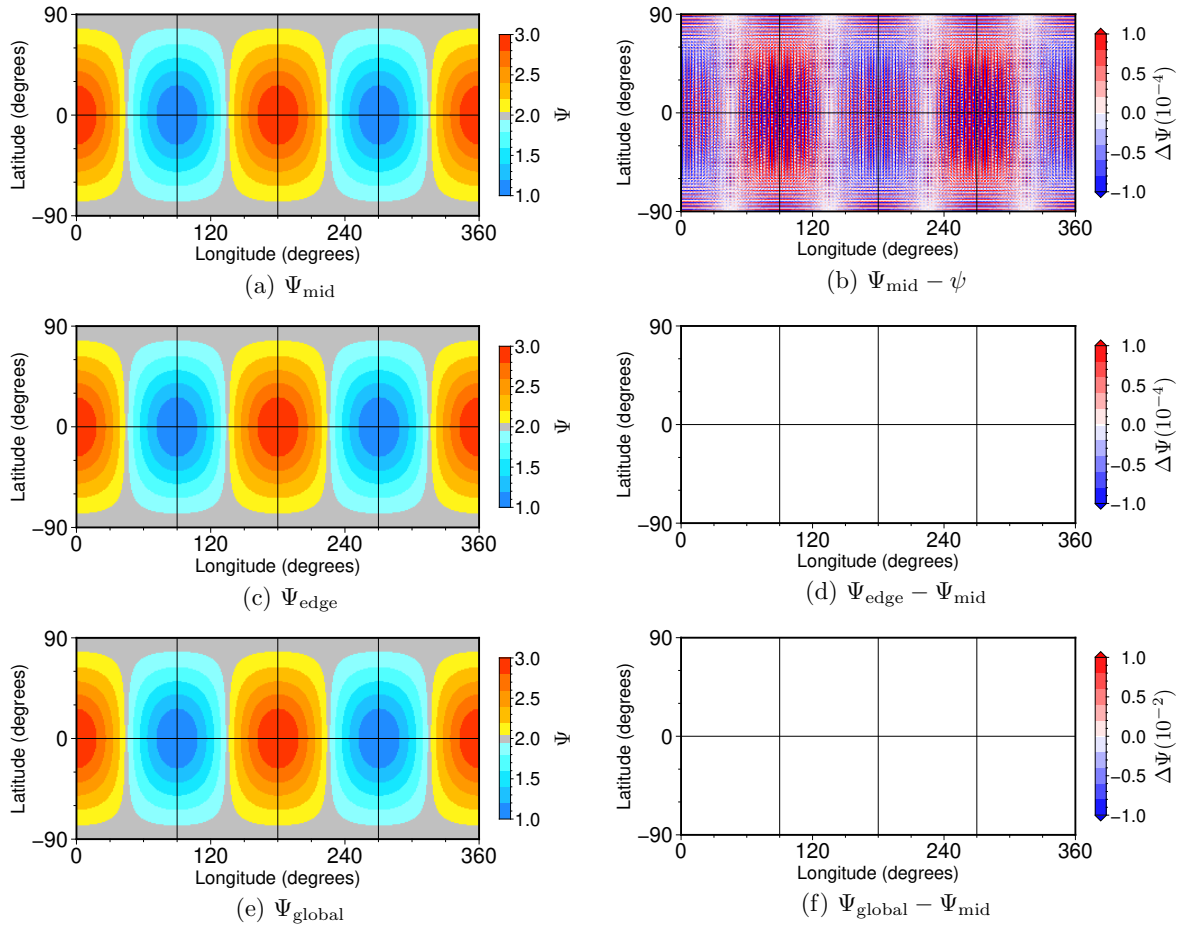

(a) $\Psi_{\rm mid}$ (b) $\Psi_{\rm mid} - \psi$

(c) $\Psi_{\rm edge}$ (d) $\Psi_{\rm edge} - \Psi_{\rm mid}$

(e) $\Psi_{\rm global}$ (f) $\Psi_{\rm global} - \Psi_{\rm mid}$

Figure S18: The same as Fig. (S17) but resolution of the destination grid cells is $(N_\theta, N_\phi) = (180, 360)$.

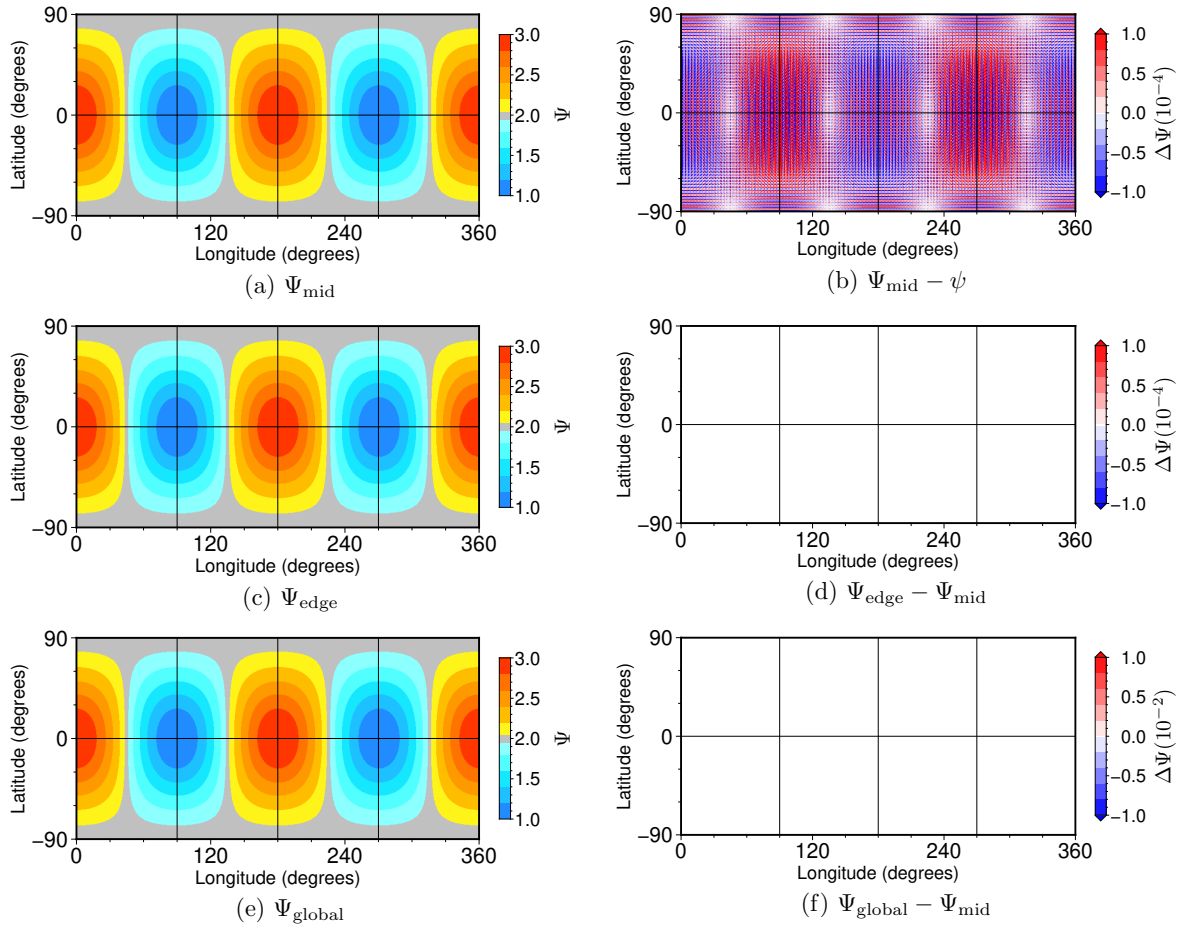

(a) Ψ_{mid} (b) $\Psi_{\mathrm{mid}} - \psi$

(c) Ψ_{edge} (d) $\Psi_{\mathrm{edge}} - \Psi_{\mathrm{mid}}$

(e) Ψ_{global} (f) $\Psi_{\mathrm{global}} - \Psi_{\mathrm{mid}}$

Figure S19: The same as Fig. (S17) but resolution of the destination grid cells is $(N_\theta, N_\phi) = (360, 720)$.

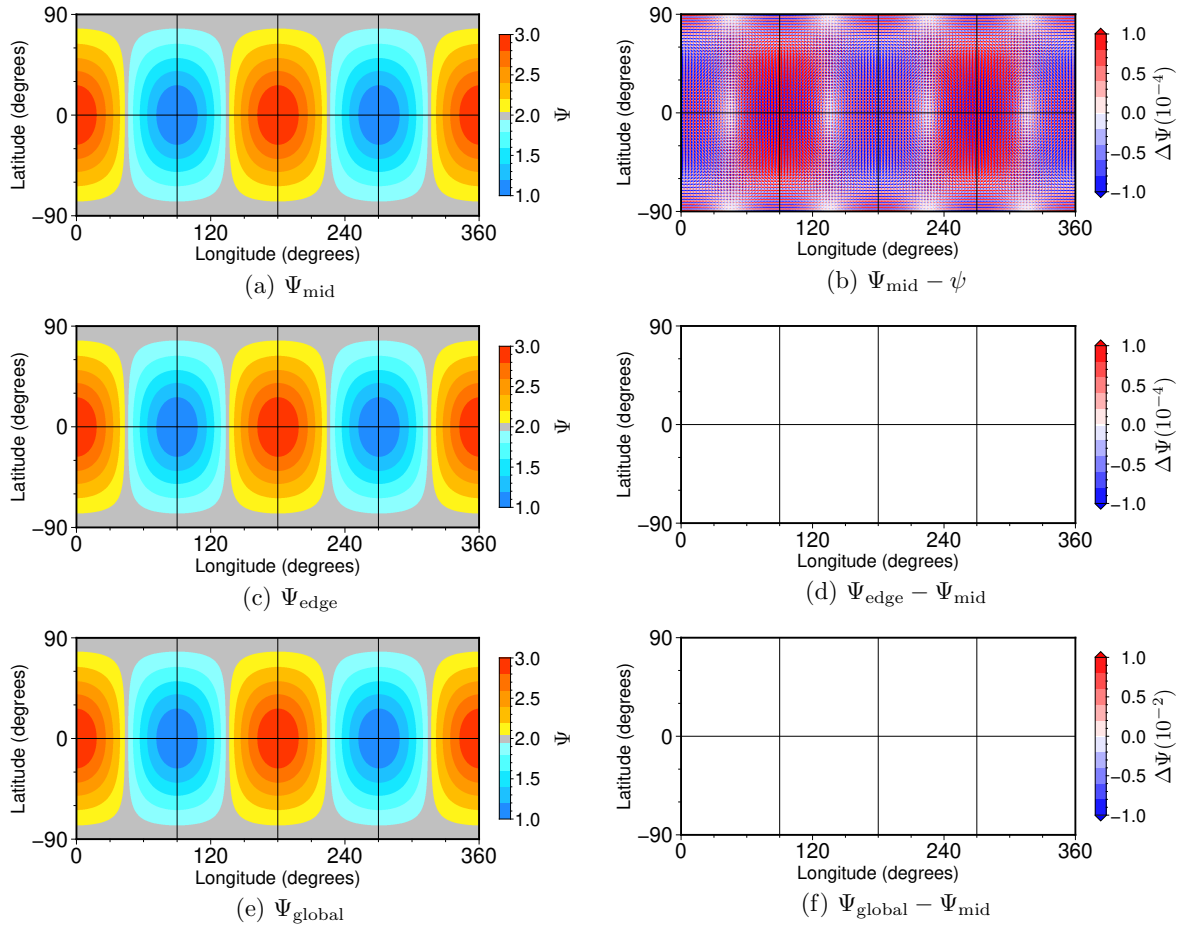

(a) $\Psi_{\rm mid}$ (b) $\Psi_{\rm mid} - \psi$

(c) $\Psi_{\rm edge}$ (d) $\Psi_{\rm edge} - \Psi_{\rm mid}$

(e) $\Psi_{\rm global}$ (f) $\Psi_{\rm global} - \Psi_{\rm mid}$

Figure S20: The same as Fig. (S17) but resolution of the destination grid cells is $(N_\theta, N_\phi) = (720, 1440)$.

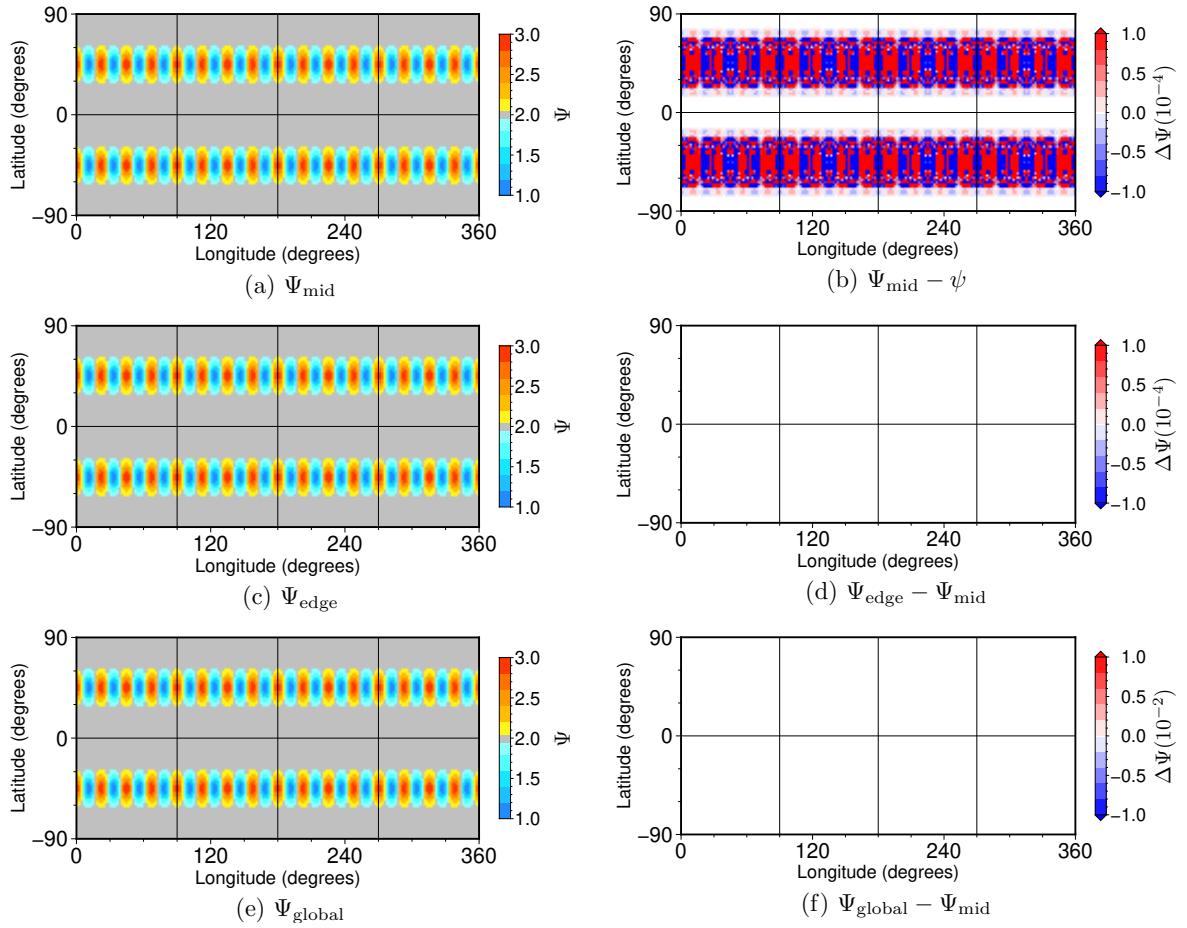

(a) Ψ_{mid} (b) $\Psi_{\mathrm{mid}} - \psi$

(c) Ψ_{edge} (d) $\Psi_{\mathrm{edge}} - \Psi_{\mathrm{mid}}$

(e) Ψ_{global} (f) $\Psi_{\mathrm{global}} - \Psi_{\mathrm{mid}}$

Figure S21: Results of sensitivity experiments A3 using Schemes P for the offset longitudes where mid, edge, global correspond to the $\phi_{\mathsf{ofs}} = (\phi_0 + \phi_1)/2$, $\phi_{\mathsf{ofs}} = \phi_1$, and $\phi_{\mathsf{ofs}} = 180^\circ$ cases, respectively. (a) One-time remapped field for mid-offset case (Ψ_{mid}). (b) Error in the remapped field of the mid-offset case ($\Psi_{\mathrm{mid}} - \psi$). (c) One-time remapped field for edge-offset case (Ψ_{edge}). (d) Difference between edge- and mid-offset cases ($\Psi_{\mathrm{edge}} - \Psi_{\mathrm{mid}}$). (e) Remapped field field for global-offset case (Ψ_{global}). (f) Difference between global- and mid-offset cases ($\Psi_{\mathrm{global}} - \Psi_{\mathrm{mid}}$). Resolution of the destination grid cells is $(N_\theta, N_\phi) = (90, 180)$.

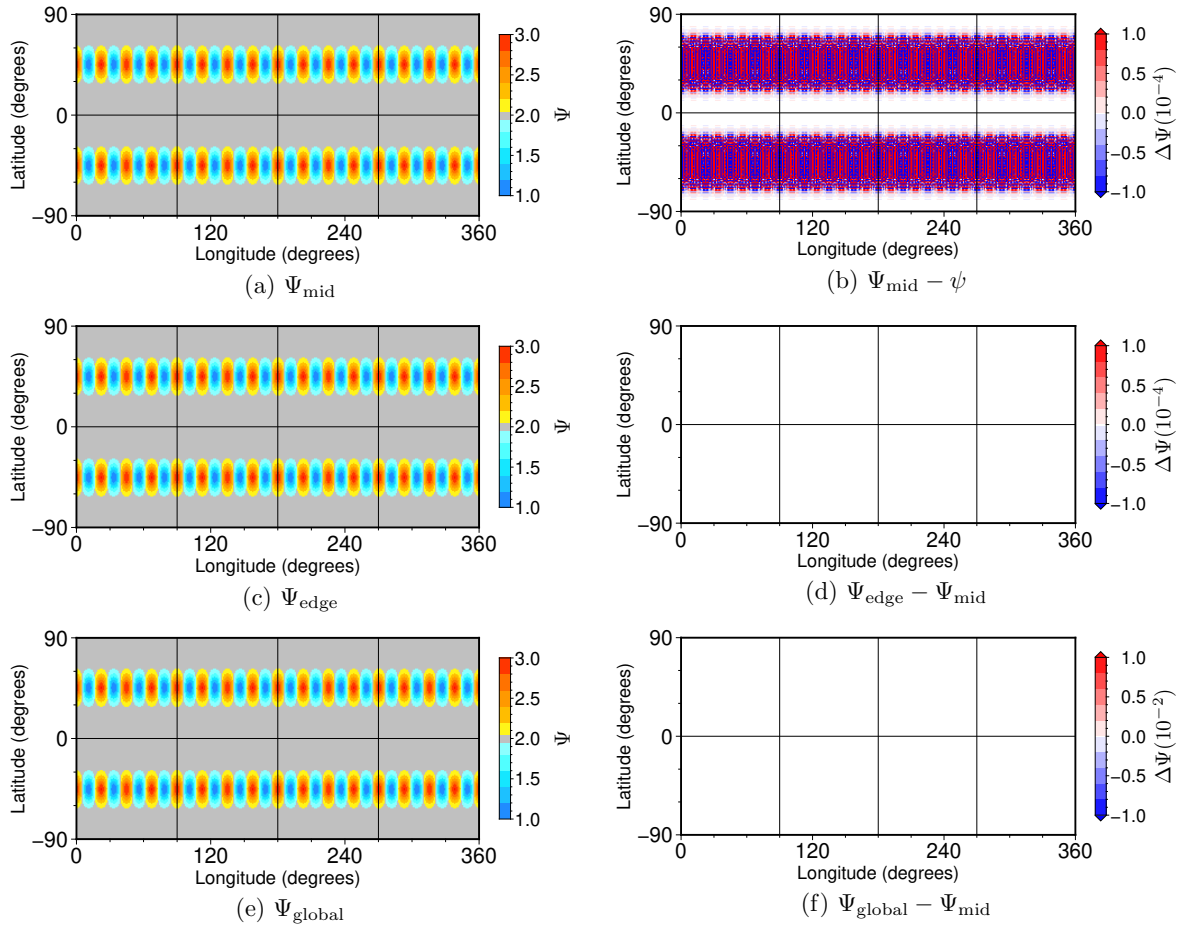

(a) Ψ_{mid} (b) $\Psi_{\mathrm{mid}} - \psi$

(c) Ψ_{edge} (d) $\Psi_{\mathrm{edge}} - \Psi_{\mathrm{mid}}$

(e) Ψ_{global} (f) $\Psi_{\mathrm{global}} - \Psi_{\mathrm{mid}}$

Figure S22: The same as Fig. (S21) but resolution of the destination grid cells is $(N_\theta, N_\phi) = (180, 360)$.

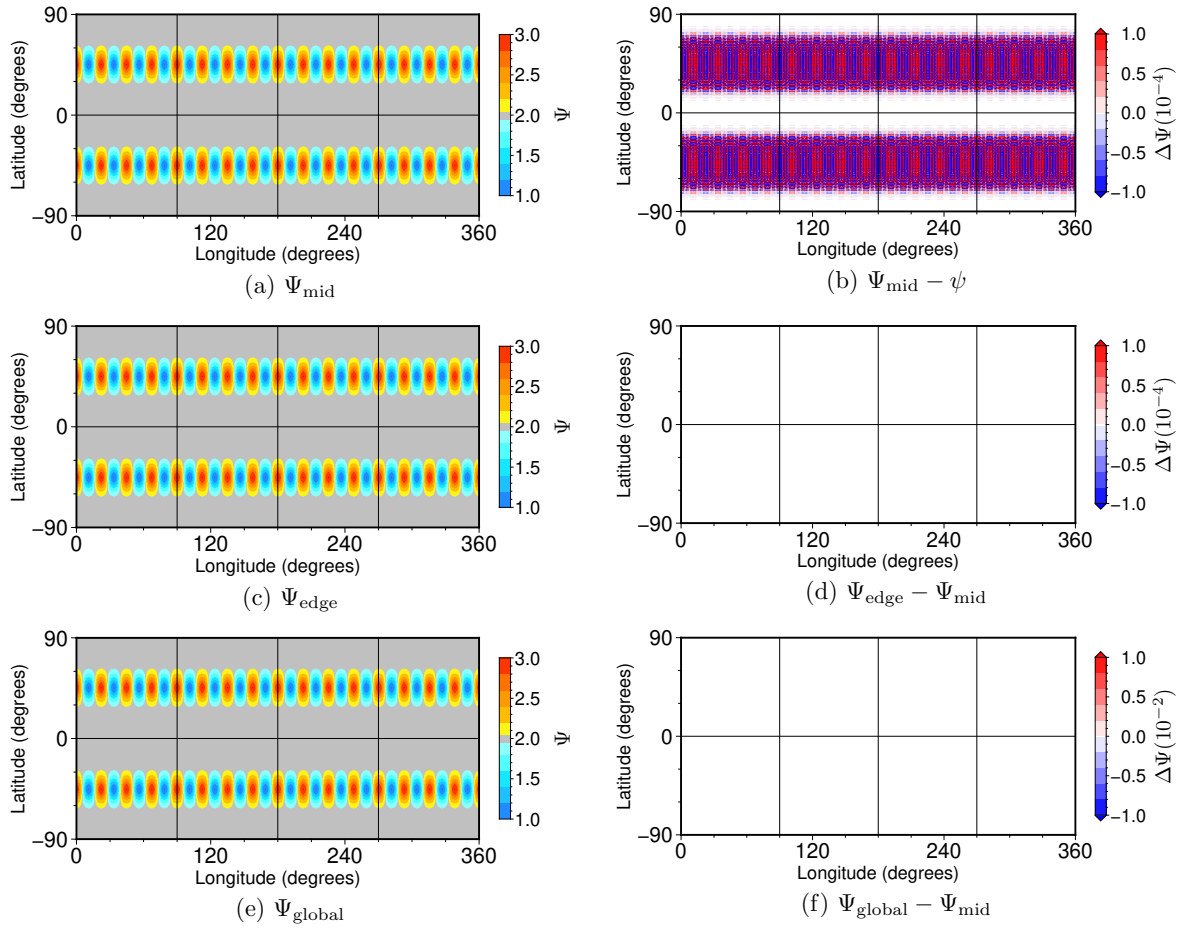

(a) Ψ_{mid} (b) $\Psi_{\mathrm{mid}} - \psi$

(c) Ψ_{edge} (d) $\Psi_{\mathrm{edge}} - \Psi_{\mathrm{mid}}$

(e) Ψ_{global} (f) $\Psi_{\mathrm{global}} - \Psi_{\mathrm{mid}}$

Figure S23: The same as Fig. (S21) but resolution of the destination grid cells is $(N_\theta, N_\phi) = (360, 720)$.

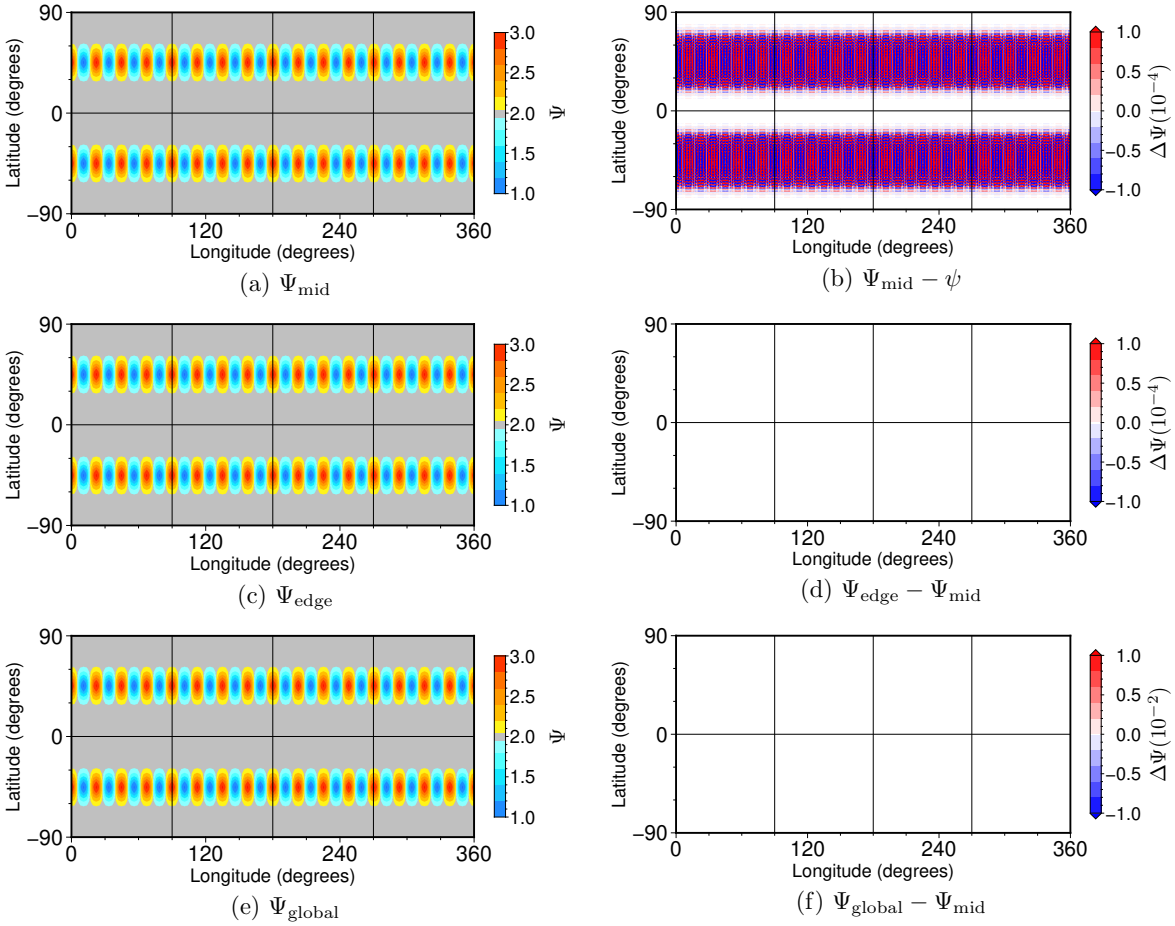

(a) Ψ_{mid} (b) $\Psi_{\mathrm{mid}} - \psi$

(c) Ψ_{edge} (d) $\Psi_{\mathrm{edge}} - \Psi_{\mathrm{mid}}$

(e) Ψ_{global} (f) $\Psi_{\mathrm{global}} - \Psi_{\mathrm{mid}}$

Figure S24: The same as Fig. (S21) but resolution of the destination grid cells is $(N_\theta, N_\phi) = (720, 1440)$.

Table S1: Summary of results of the sensitivity experiments in the paper. The absolute value of relative error in global conservation ($|L_g|$) is shown.

(a) Summary of experiment A1.

Scheme	Offset	$(90, 180)$ $[\times 10^{-15}]$	$(180, 360)$ $[\times 10^{-15}]$	$(360, 720)$ $[\times 10^{-15}]$	$(720, 1440)$ $[\times 10^{-15}]$
N	mid	0.014	0.057	0.232	0.191
N	edge	0.014	0.054	0.232	0.188
N	global	2172.	5395.	1348.	3372.
P	mid	0.010	0.058	0.232	0.191
P	edge	0.019	0.058	0.231	0.191
P	global	0.066	0.172	0.132	0.254

(b) Summary of experiment A2.

Scheme	Offset	$(90, 180)$ $[\times 10^{-15}]$	$(180, 360)$ $[\times 10^{-15}]$	$(360, 720)$ $[\times 10^{-15}]$	$(720, 1440)$ $[\times 10^{-15}]$
N	mid	0.141	0.141	0000.	0.565
N	edge	0.141	0000.	0.282	0000.
N	global	8189.	2034.	5086.	1271.
P	mid	0.282	0.141	0000.	0.565
P	edge	0.141	0.141	0000.	0.565
P	global	0.141	0000.	0000.	0.565

(c) Summary of experiment A3.

Scheme	Offset	$(90, 180)$ $[\times 10^{-15}]$	$(180, 360)$ $[\times 10^{-15}]$	$(360, 720)$ $[\times 10^{-15}]$	$(720, 1440)$ $[\times 10^{-15}]$
N	mid	2.120	1.696	4.240	6.785
N	edge	2.120	1.696	2.827	6.643
N	global	5834.	1440.	3613.	9040.
P	mid	2.120	1.696	4.240	6.785
P	edge	2.120	1.554	4.240	6.785
P	global	1.979	1.696	3.675	6.785

Table S2: The same as Tab. S1 but for metric $\|E\|_{L_2}$.

(a) Summary of experiment A1.

Scheme	Offset	$(90, 180)$ $[\times 10^{-5}]$	$(180, 360)$ $[\times 10^{-5}]$	$(360, 720)$ $[\times 10^{-6}]$	$(720, 1440)$ $[\times 10^{-7}]$
N	mid	2.687417	6.668807	8.670443	9.651116
N	edge	**3.064012**	**7.471429**	**9.675760**	**10.76568**
N	global	**107.0940**	**245.1191**	**312.4807**	**347.0928**
P	mid	2.687417	6.668807	8.670443	9.651116
P	edge	(*14d*)	6.668807	(*14d*)	(*14d*)
P	global	(*12d*)	(*12d*)	(*12d*)	(*13d*)

(b) Summary of experiment A2.

Scheme	Offset	$(90, 180)$ $[\times 10^{-5}]$	$(180, 360)$ $[\times 10^{-6}]$	$(360, 720)$ $[\times 10^{-7}]$	$(720, 1440)$ $[\times 10^{-7}]$
N	mid	3.570240	8.250488	1.016097	1.090981
N	edge	**4.331781**	**9.979499**	1.**243238**	1.**350379**
N	global	**177.8254**	**406.9487**	**51.92524**	**57.68116**
P	mid	3.570240	8.250488	1.016097	1.090981
P	edge	(*13d*)	(*13d*)	1.016097	(*14d*)
P	global	(*12d*)	(*12d*)	(*13d*)	(*13d*)

(c) Summary of experiment A3.

Scheme	Offset	$(90, 180)$ $[\times 10^{-5}]$	$(180, 360)$ $[\times 10^{-6}]$	$(360, 720)$ $[\times 10^{-6}]$	$(720, 1440)$ $[\times 10^{-6}]$
N	mid	1.348668	3.149976	4.191737	4.636039
N	edge	1.3**63358**	3.1**83171**	4.**229582**	4.6**77910**
N	global	**14.80939**	**34.02213**	**41.91800**	**46.36844**
P	mid	1.348668	3.149976	4.191737	4.636039
P	edge	1.348668	(*14d*)	4.191737	4.636039
P	global	(*13d*)	(*13d*)	(*14d*)	(*13d*)

Table S3: The same as Tab. S1 but for metric $\|E\|_{L_\infty}$.

(a) Summary of experiment A1.

Scheme	Offset	$(90, 180)$ $[\times 10^{-5}]$	$(180, 360)$ $[\times 10^{-5}]$	$(360, 720)$ $[\times 10^{-6}]$	$(720, 1440)$ $[\times 10^{-6}]$
N	mid	4.944287	1.083916	1.958858	2.538128
N	edge	**5.071775**	1.08**8965**	1.9**69803**	2.5**67481**
N	global	**252.1286**	**67.23952**	**86.01129**	**95.42889**
P	mid	4.944287	1.083916	1.958858	2.538128
P	edge	(*12d*)	(*13d*)	(*15d*)	(*15d*)
P	global	(*11d*)	(*11d*)	(*13d*)	(*13d*)

(b) Summary of experiment A2.

Scheme	Offset	$(90, 180)$ $[\times 10^{-5}]$	$(180, 360)$ $[\times 10^{-6}]$	$(360, 720)$ $[\times 10^{-7}]$	$(720, 1440)$ $[\times 10^{-7}]$
N	mid	9.530795	1.963583	2.913715	3.342430
N	edge	9.5**75834**	**2.172476**	**3.084127**	3.**642582**
N	global	**477.2723**	**128.6125**	**164.5735**	**182.6903**
P	mid	9.530795	1.963583	2.913715	3.342430
P	edge	(*15d*)	(*11d*)	(*15d*)	(*12d*)
P	global	(*11d*)	(*11d*)	(*11d*)	(*12d*)

(c) Summary of experiment A3.

Scheme	Offset	$(90, 180)$ $[\times 10^{-5}]$	$(180, 360)$ $[\times 10^{-5}]$	$(360, 720)$ $[\times 10^{-6}]$	$(720, 1440)$ $[\times 10^{-5}]$
N	mid	4.687224	1.012223	1.626061	1.987591
N	edge	4.**730911**	1.**147515**	1.**761587**	**2.135815**
N	global	**80.95277**	**21.55330**	**28.27784**	**31.38418**
P	mid	4.687224	1.012223	1.626061	1.987591
P	edge	(*12d*)	(*13d*)	(*12d*)	(*13d*)
P	global	(*11d*)	(*11d*)	(*11d*)	(*9d*)

Table S4: The same as Tab. S1 but for metric $\|E\|_{H_1}$.

(a) Summary of experiment A1.

Scheme	Offset	$(90, 180)$ $[\times 10^{-4}]$	$(180, 360)$ $[\times 10^{-5}]$	$(360, 720)$ $[\times 10^{-5}]$	$(720, 1440)$ $[\times 10^{-5}]$
N	mid	8.160238	3.551862	1.086087	1.740331
N	edge	**9.073365**	3.**872535**	1.**167091**	1.**880009**
N	global	**288.6347**	**112.2963**	**31.09290**	**51.75169**
P	mid	8.160238	3.551862	1.086087	1.740331
P	edge	(*14d*)	(*13d*)	(*13d*)	(*14d*)
P	global	(*12d*)	(*11d*)	(*13d*)	(*11d*)

(b) Summary of experiment A2.

Scheme	Offset	$(90, 180)$ $[\times 10^{-5}]$	$(180, 360)$ $[\times 10^{-5}]$	$(360, 720)$ $[\times 10^{-6}]$	$(720, 1440)$ $[\times 10^{-6}]$
Scheme	Offset	$(90, 180)$ $[\times 10^{-3}]$	$(180, 360)$ $[\times 10^{-3}]$	$(360, 720)$ $[\times 10^{-2}]$	$(720, 1440)$ $[\times 10^{-2}]$
N	mid	1.056206	4.232089	1.226052	1.829100
N	edge	1.**245376**	4.**949951**	1.**417992**	**2.179947**
N	global	**47.83382**	**186.1344**	**51.64459**	**85.97318**
P	mid	1.056206	4.232089	1.226052	1.829100
P	edge	(*12d*)	(*12d*)	(*13d*)	(*13d*)
P	global	(*12d*)	(*12d*)	(*13d*)	(*11d*)

(c) Summary of experiment A3.

Scheme	Offset	$(90, 180)$ $[\times 10^{-4}]$	$(180, 360)$ $[\times 10^{-4}]$	$(360, 720)$ $[\times 10^{-4}]$	$(720, 1440)$ $[\times 10^{-4}]$
N	mid	4.190114	1.614821	6.109832	1.003218
N	edge	4.**243329**	1.6**32635**	6.1**38378**	1.00**7971**
N	global	**48.94886**	**17.73452**	**43.97683**	**7.272782**
P	mid	4.190114	1.614821	6.109832	1.003218
P	edge	(*14d*)	(*14d*)	6.109832	1.003218
P	global	(*12d*)	(*13d*)	(*13d*)	(*13d*)

Table S5: The same as Tab. S1 but for metric $|L_g|$ after 1000-time iterative remapping.

(a) Summary of experiment A1.

Scheme	Offset	$(90, 180)$ $[\times 10^{-15}]$	$(180, 360)$ $[\times 10^{-15}]$	$(360, 720)$ $[\times 10^{-15}]$	$(720, 1440)$ $[\times 10^{-15}]$
N	mid	67.98	464.1	27.70	43.86
N	edge	93.79	474.2	32.54	43.81
N	global	6308.	3773.	∞	∞
P	mid	23.87	440.4	17.25	51.03
P	edge	82.69	395.1	42.87	43.68
P	global	37.18	549.6	188.8	355.0

(b) Summary of experiment A2.

Scheme	Offset	$(90, 180)$ $[\times 10^{-15}]$	$(180, 360)$ $[\times 10^{-15}]$	$(360, 720)$ $[\times 10^{-15}]$	$(720, 1440)$ $[\times 10^{-15}]$
N	mid	227.3	1388.	103.0	150.1
N	edge	76.33	1458.	52.72	136.2
N	global	2392.	4327.	∞	∞
P	mid	269.2	1372.	34.06	149.5
P	edge	325.9	1400.	17.52	134.0
P	global	43.25	1519.	25.86	134.2

(c) Summary of experiment A3.

Scheme	Offset	$(90, 180)$ $[\times 10^{-15}]$	$(180, 360)$ $[\times 10^{-15}]$	$(360, 720)$ $[\times 10^{-15}]$	$(720, 1440)$ $[\times 10^{-15}]$
N	mid	138.9	1306.	123.6	132.7
N	edge	22.89	1369.	76.75	115.9
N	global	1683.	1638.	∞	∞
P	mid	224.3	1292.	57.10	132.1
P	edge	255.4	1318.	36.32	113.5
P	global	34.49	1428.	53.57	121.2

Table S6: The same as Tab. S2 but for metric $\|E\|_{L_2}$ after 1000-time iterative remapping.

(a) Summary of experiment A1.

Scheme	Offset	$(90, 180)$ $[\times 10^{-4}]$	$(180, 360)$ $[\times 10^{-4}]$	$(360, 720)$ $[\times 10^{-5}]$	$(720, 1440)$ $[\times 10^{-5}]$
N	mid	5.529522	1.141016	8.849167	1.984378
N	edge	5.529**917**	1.14**8703**	**9.173183**	**3.845315**
N	global	**90821.45**	∞	∞	∞
P	mid	5.529522	1.141016	8.849167	1.984378
P	edge	(*9d*)	(*9d*)	(*10d*)	(*10d*)
P	global	(*9d*)	(*10d*)	(*8d*)	(*10d*)

(b) Summary of experiment A2.

Scheme	Offset	$(90, 180)$ $[\times 10^{-5}]$	$(180, 360)$ $[\times 10^{-5}]$	$(360, 720)$ $[\times 10^{-5}]$	$(720, 1440)$ $[\times 10^{-6}]$
N	mid	3.404520	1.242931	1.153953	2.549738
N	edge	3.40**6271**	1.2**61852**	1.**221960**	**6.049095**
N	global	**121409.7**	∞	∞	∞
P	mid	3.404520	1.242931	1.153953	2.549738
P	edge	(*7d*)	(*10d*)	(*10d*)	(*9d*)
P	global	(*8d*)	(*8d*)	(*9d*)	(*9d*)

(c) Summary of experiment A3.

Scheme	Offset	$(90, 180)$ $[\times 10^{-2}]$	$(180, 360)$ $[\times 10^{-3}]$	$(360, 720)$ $[\times 10^{-4}]$	$(720, 1440)$ $[\times 10^{-4}]$
N	mid	2.542678	3.742836	5.796647	1.050506
N	edge	(*7d*)	3.742**923**	5.**812058**	1.**164832**
N	global	2.**786510**	∞	∞	∞
P	mid	2.542678	3.742836	5.796647	1.050506
P	edge	(*11d*)	(*10d*)	(*8d*)	(*11d*)
P	global	(*12d*)	(*10d*)	(*8d*)	(*10d*)

Table S7: The same as Tab. S3 but for metric $\|E\|_{L_\infty}$ after 1000-time iterative remapping.

(a) Summary of experiment A1.

Scheme	Offset	$(90, 180)$ $[\times 10^{-3}]$	$(180, 360)$ $[\times 10^{-4}]$	$(360, 720)$ $[\times 10^{-4}]$	$(720, 1440)$ $[\times 10^{-5}]$
N	mid	1.143672	1.976176	1.849959	4.872257
N	edge	1.14**5761**	1.97**7551**	1.8**50817**	**10.42006**
N	global	**591567.4**	**2516259.**	∞	∞
P	mid	1.143672	1.976176	1.849959	4.872257
P	edge	(*12d*)	(*7d*)	(*8d*)	(*7d*)
P	global	(*11d*)	(*8d*)	(*9d*)	(*7d*)

(b) Summary of experiment A2.

Scheme	Offset	$(90, 180)$ $[\times 10^{-5}]$	$(180, 360)$ $[\times 10^{-5}]$	$(360, 720)$ $[\times 10^{-5}]$	$(720, 1440)$ $[\times 10^{-6}]$
N	mid	7.229935	2.836765	3.495363	8.932623
N	edge	7.**337693**	2.83**9733**	3.**505998**	**21.10220**
N	global	**1227662.**	**5312862.**	∞	∞
P	mid	7.229935	2.836765	3.495363	8.932623
P	edge	(*7d*)	(*8d*)	(*10d*)	(*7d*)
P	global	(*7d*)	(*9d*)	(*8d*)	(*7d*)

(c) Summary of experiment A3.

Scheme	Offset	$(90, 180)$ $[\times 10^{-2}]$	$(180, 360)$ $[\times 10^{-2}]$	$(360, 720)$ $[\times 10^{-3}]$	$(720, 1440)$ $[\times 10^{-4}]$
N	mid	7.739175	1.106519	2.235436	5.166085
N	edge	7.739**280**	1.1065**20**	2.2**90092**	**6.569416**
N	global	**8.024978**	**7186866.**	∞	∞
P	mid	7.739175	1.106519	2.235436	5.166085
P	edge	(*10d*)	(*9d*)	(*10d*)	(*9d*)
P	global	(*10d*)	(*9d*)	(*8d*)	(*7d*)

Table S8: The same as Tab. S4 but for metric $\|E\|_{H_1}$ after 1000-time iterative remapping.

(a) Summary of experiment A1.

Scheme	Offset	$(90, 180)$ $[\times 10^{-2}]$	$(180, 360)$ $[\times 10^{-3}]$	$(360, 720)$ $[\times 10^{-3}]$	$(720, 1440)$ $[\times 10^{-3}]$
N	mid	1.156071	3.635854	8.923197	3.487481
N	edge	1.156**152**	3.6**57658**	**9.127597**	**5.592652**
N	global	**927295.6**	∞	∞	∞
P	mid	1.156071	3.635854	8.923197	3.487481
P	edge	(*12d*)	(*9d*)	(*11d*)	(*10d*)
P	global	(*7d*)	(*8d*)	(*8d*)	(*8d*)

(b) Summary of experiment A2.

Scheme	Offset	$(90, 180)$ $[\times 10^{-4}]$	$(180, 360)$ $[\times 10^{-4}]$	$(360, 720)$ $[\times 10^{-3}]$	$(720, 1440)$ $[\times 10^{-4}]$
N	mid	7.290697	4.128391	1.173717	4.511081
N	edge	7.29**4201**	4.1**79597**	1.**216562**	**8.569447**
N	global	**1239478**.	∞	∞	∞
P	mid	7.290696	4.128392	1.173717	4.511081
P	edge	(*7d*)	4.12839**3**	(*9d*)	(*8d*)
P	global	(*7d*)	4.12839**3**	(*7d*)	(*7d*)

(c) Summary of experiment A3.

Scheme	Offset	$(90, 180)$ $[\times 10^{-1}]$	$(180, 360)$ $[\times 10^{-1}]$	$(360, 720)$ $[\times 10^{-2}]$	$(720, 1440)$ $[\times 10^{-2}]$
N	mid	5.996567	1.098501	5.243229	2.025716
N	edge	5.99656**8**	1.09854**8**	5.2**53945**	2.**132798**
N	global	**7.093377**	∞	∞	∞
P	mid	5.996567	1.098501	5.243229	2.025716
P	edge	(*10d*)	(*12d*)	(*10d*)	(*10d*)
P	global	(*11d*)	(*11d*)	(*11d*)	(*9d*)

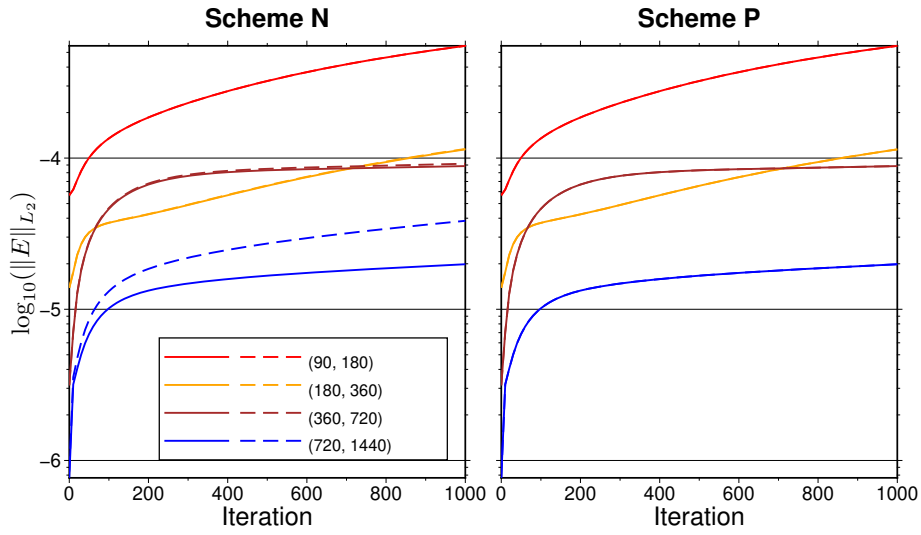

(a) $\|E\|_{L_2}$

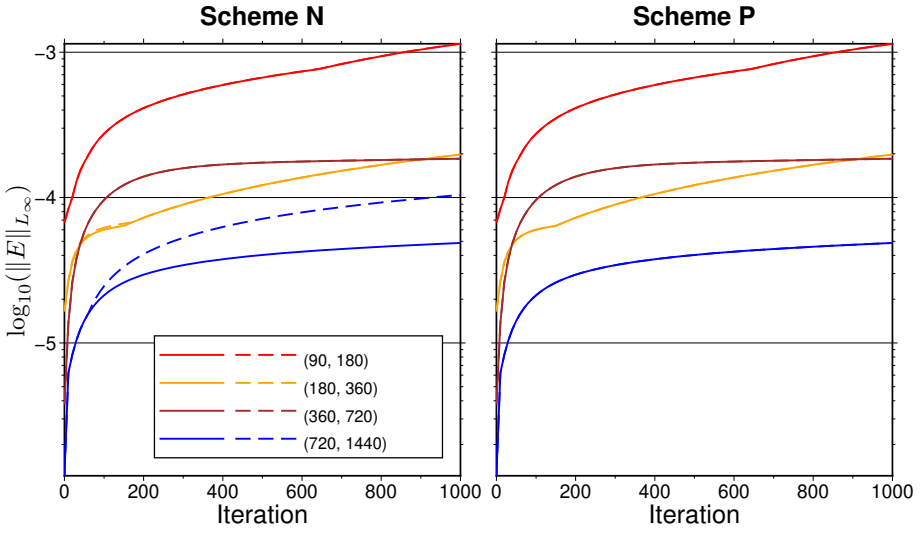

(b) $\|E\|_{L_\infty}$

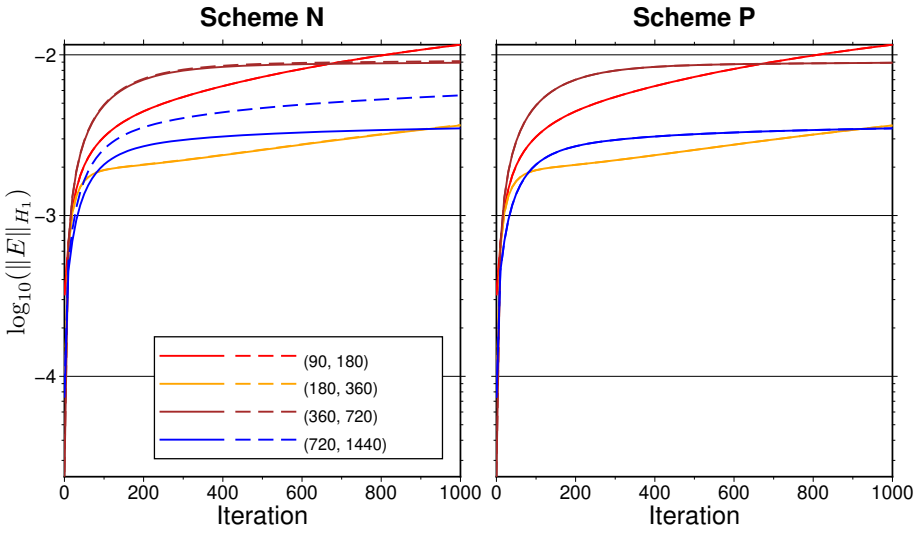

(c) $\|E\|_{H_1}$

Figure S25: Results of the sensitivity experiments A1 for the offset longitude using Schemes N and P. Destination grid sizes are $(N_\theta, N_\phi) = (90, 180)$, $(180, 360)$, $(360, 720)$, $(720, 1440)$. Solid and dashed lines indicate that $\phi_{\mathsf{ofs}} = (\phi_0 + \phi_1)/2$ and $\phi_{\mathsf{ofs}} = \phi_1$ cases, respectively, and mostly they are overlapped except for some particular cases. Global offset cases ($\phi_{\mathsf{ofs}} = 180°$) are excluded from the plot, because the metrics explode at early stage for Scheme N, and because the metrics overlaps with other cases for Scheme P. The metric $\|E\|_{L_2}$ as a function of iteration number of two-way remapping is shown.

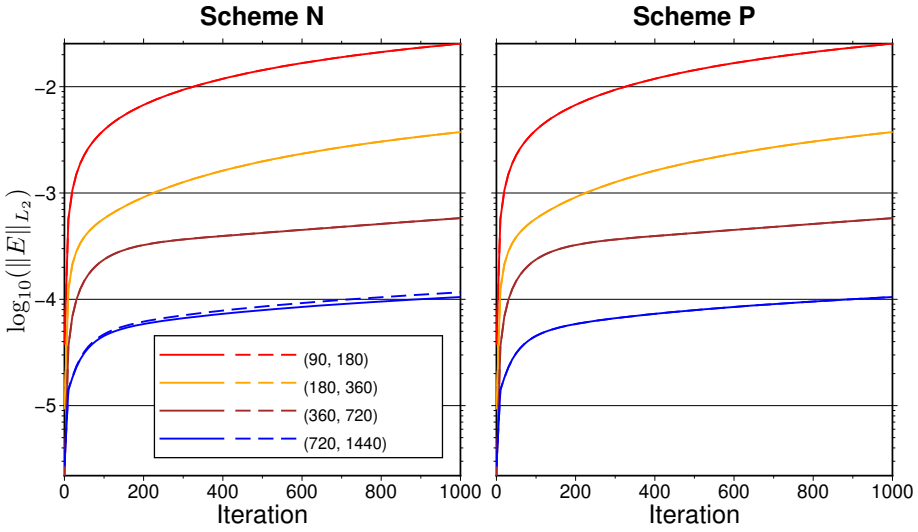

(a) $\|E\|_{L_2}$

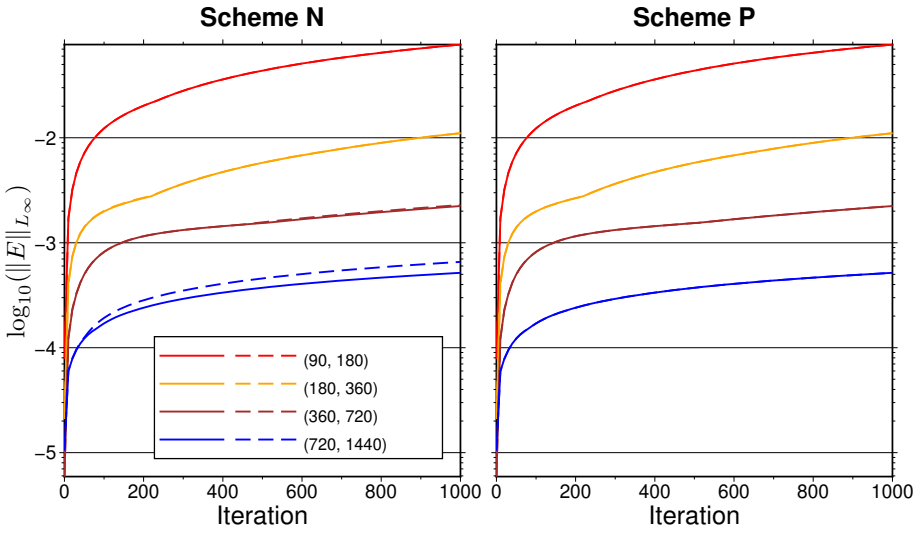

(b) $\|E\|_{L_\infty}$

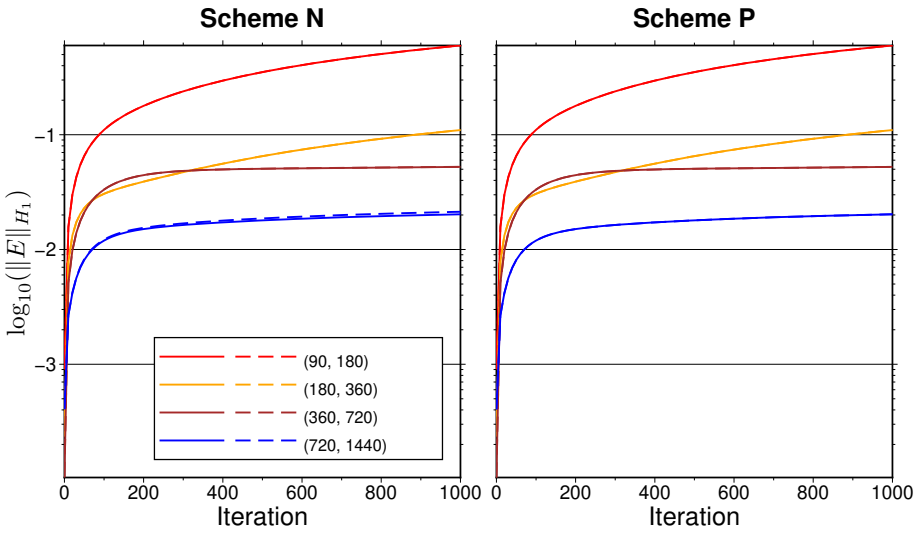

(c) $\|E\|_{H_1}$

Figure S26: The same as Fig. S25 but for experiment A3.

References

Chen, H., Ullrich, P. A., Panetta, J., Marsico, D., Hanke, M., Jain, R., Zhang, C., and Jacob, R. L.: Accurate and Robust Geometric Algorithms for Regridding on the Sphere, EGUsphere, 2026, 1–40, https://doi.org/10.5194/egusphere-2026-636, 2026.

Dukowicz, J. K. and Kodis, J. W.: Accurate Conservative Remapping (Rezoning) for Arbitrary Lagrangian-Eulerian Computations, SIAM Journal on Scientific and Statistical Computing, 8, 305–321, https://doi.org/10.1137/0908037, 1987.

Hanke, M., Redler, R., Holfeld, T., and Yastremsky, M.: YAC 1.2.0: new aspects for coupling software in Earth system modelling, Geosci. Model Dev., 9, 2755–2769, https://doi.org/10.5194/gmd-9-2755-2016, 2016.

Jones, P. W.: First- and Second-Order Conservative Remapping Schemes for Grids in Spherical Coordinates, Monthly Weather Review, 127, 2204 – 2210, https://doi.org/10.1175/1520-0493(1999)127⟨2204:FASOCR⟩2.0.CO;2, 1999.

Jones, P. W.: Comment on egusphere-2024-1101, `https://doi.org/10.5194/egusphere-2024-1101-RC2`, 2024.

Ullrich, P. A. and Taylor, M. A.: Arbitrary-Order Conservative and Consistent Remapping and a Theory of Linear Maps: Part I, Monthly Weather Review, 143, 2419 – 2440, https://doi.org/10.1175/MWR-D-14-00343.1, 2015.

Ullrich, P. A., Lauritzen, P. H., and Jablonowski, C.: Geometrically Exact Conservative Remapping (GECoRe): Regular Latitude–Longitude and Cubed-Sphere Grids, Monthly Weather Review, 137, 1721 – 1741, https://doi.org/10.1175/2008MWR2817.1, 2009.

Ullrich, P. A., Devendran, D., and Johansen, H.: Arbitrary-Order Conservative and Consistent Remapping and a Theory of Linear Maps: Part II, Monthly Weather Review, 144, 1529 – 1549, https://doi.org/10.1175/MWR-D-15-0301.1, 2016.